
A Regime Theory of Controller Class Selection for LLM Action Decisions

Zhaoyang Jiang

University of Glasgow
3167645J@student.gla.ac.uk

Zhizhong Fu

UESTC, Chengdu, China
zhizhong.fu@std.uestc.edu.cn

Yunsoo Kim

University College London
yunsoo.kim.23@ucl.ac.uk

Jiacong Mi

University of Glasgow
j.mi.1@research.gla.ac.uk

Zicheng Li

University of Glasgow
3222974L@student.gla.ac.uk

Xuanqi Peng

University of Glasgow
3131960P@student.gla.ac.uk

Honghan Wu*

University of Glasgow
Honghan.Wu@glasgow.ac.uk

Abstract

Deployed language and vision-language models must decide, on each input, whether to answer directly, retrieve evidence, defer to a stronger model, or abstain. Contrary to the common monotonicity intuition, greater per-input expressivity is not uniformly beneficial in finite samples: under identical strict cross-validation, different benchmarks prefer different controller classes. This reflects a finite-sample limitation of instance-level uncertainty signals, which can be exhausted at a distribution-dependent scale. We organize controllers into a nested lattice of four classes: fixed actions, partition routers, instance-level controllers, and prior-gated controllers, ordered by complexity. We prove a regime theory that turns three data-estimable bottlenecks into a class choice: how much improvement is possible beyond the best fixed action, whether there are enough samples for instance-level controllers to make reliable decisions, and how much improvement a coarse partition router can recover when instance-level signal is unreliable. The resulting Bernstein-tight threshold has a matching information-theoretic lower bound, and strict nested cross-validation provably selects a near-best class. Across SMS-Spam, HallusionBench, A-OKVQA, and FOLIO, the predicted class matches the empirical winner; the prior-gated controller wins on TextVQA when OCR tokens supply a label-free prediction-time prior. Code is available at <https://github.com/Anonymous-Awesome-Submissions/Regime-Theory>.

*Corresponding author.

1 Introduction

Consider a medical question-answering system in clinical use. When asked “what does this chest X-ray show?”, the system has several options: answer directly, retrieve relevant prior cases first, defer to a stronger specialist model, or abstain. A system that always answers, even when uncertain, is not just less accurate; it is dangerous. As large language and vision-language models move from benchmarks into deployment, *when* to answer is becoming as consequential as *how*. A confidently wrong diagnosis, a fluent but factually incorrect claim, or a hard query handled by a weak model when a stronger one was available all share a common cause: the system chose the wrong action for an uncertain input.

The standard engineering response is to put a *controller* in front of the model, with each subliteration settling on its own fixed structural design. The earliest version of the controller idea is the reject option: when confidence is too low, the system refuses to predict [Chow, 2003, El-Yaniv et al., 2010, Geifman and El-Yaniv, 2017]. The same logic reappears across modern generation systems as a decision to retrieve evidence before answering [Lewis et al., 2020, Karpukhin et al., 2020, Izacard et al., 2023], to pass a hard case to a stronger expert [Mozannar and Sontag, 2020, Narasimhan et al., 2022, Verma et al., 2023, Mao et al., 2023], or to climb a cost-ordered cascade of models [Chen et al., 2023, Jitkrittum et al., 2023, Ding et al., 2024, Ong et al., 2024, Dekoninck et al., 2024]. What changes across these settings is the action set and the surrogate; the underlying object is the same: a controller that maps each input to an action. Each subliteration then fixes, in advance, how expressive that map is allowed to be (for example, a global threshold, a calibrated selective score, an instance-level learned rule, or a cascade router), and optimizes within that fixed family, without asking whether the data support a coarser or finer controller class.

Our results contradict the implicit monotonicity premise in a structured way. Under an identical strict cross-validation protocol, the winning controller class changes with the statistical regime of the benchmark. On HallusionBench [Guan et al., 2024] and A-OKVQA [Schwenk et al., 2022], instance-level learned controllers win, consistent with strong per-sample signal and enough data to estimate it. On FOLIO [Han et al., 2024], the sample size is far below the finite-sample viability threshold for instance-level control; a partition router reduces loss, while the best instance-level controller is slightly worse than the best fixed action. On SMS-Spam, the best fixed action already leaves very few inputs on which any alternative action can improve, and it remains the empirical winner (full numbers in Table 1). Thus the finite-sample ordering is not monotone in controller complexity: a coarser class can be the statistically justified choice even when a finer per-input rule is available. Two canonical cost-sensitive learning-to-defer baselines [Mozannar and Sontag, 2020, Narasimhan et al., 2022], both instance-level by construction, recover the high-signal gains on HallusionBench and A-OKVQA but fall behind the partition router on FOLIO. The effect is therefore about controller class, not a peculiarity of our implementation: the right question is not how to make the controller more expressive everywhere, but which class the data can actually support.

Two recent results suggest why. Jitkrittum et al. [2023] show that confidence-based cascade deferral is Bayes-optimal only when instance-level confidence is a sufficient statistic; Kalai and Vempala [2024] and Karbasi et al. [2025] prove impossibility-style lower bounds for hallucination detection from instance-level information alone. Both point to the same constraint: *instance-level information is exhausted at a finite, distribution-dependent scale*. Neither, however, says how to choose a controller in practice. The question we therefore answer is: *given the data, which controller class is statistically justified?*

We organize controllers into a strictly nested four-class lattice $\Pi_0 \subset \Pi_1 \subset \Pi_2 \subset \Pi_3$ (Figure 1): fixed actions, partition routers that split inputs into a few groups, instance-level learned controllers, and prior-gated controllers that use an external signal when it is confident and otherwise fall back to a lower-class controller. The statistical point is simple: more complex controllers require enough samples before their gains can be certified, but passing this viability test does not by itself make a class the right choice. At a given (D, n) we should use the class whose certified gain best exceeds its estimation cost, which can be a lower-complexity class even when a higher one is statistically viable.

The theory makes this class choice operational. It reduces the question “which controller class should be used at this data scale?” to three data-estimable bottlenecks: whether there is enough residual mass for any adaptive controller to improve beyond the best fixed action, whether the available sample size can certify the sign of an instance-level Π_2 gain, and whether stable group-level action gaps

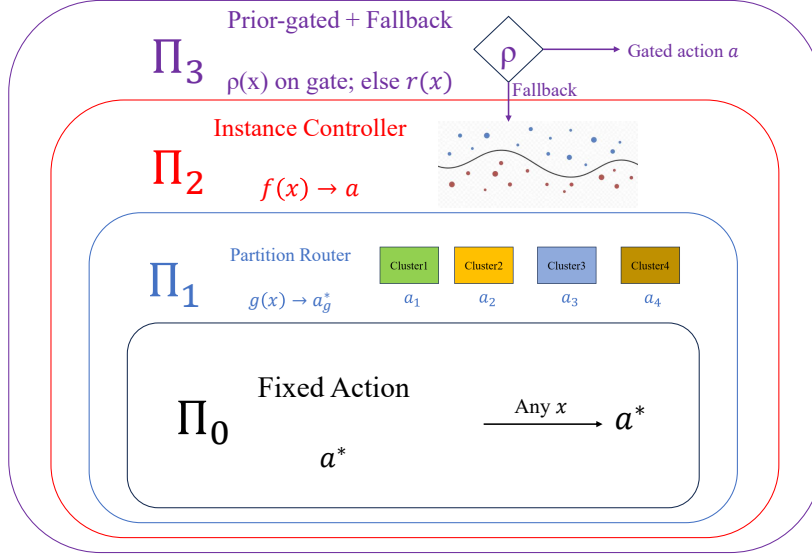


Figure 1: The nested lattice of policy classes. Π_0 contains fixed actions; Π_1 contains partition routers; Π_2 contains instance-level learned controllers; Π_3 pairs a deterministic prior gate with a fallback controller drawn from a lower class.

allow a coarser Π_1 router to recover loss when per-sample control is unreliable. These bottlenecks are formalized by the residual bound, the Bernstein-tight Π_2 viability threshold with a matching information-theoretic lower bound, and the partition-gain bound (Theorems 1–3, Proposition 1). Strict nested cross-validation then turns the diagnostics into a selection rule, choosing a near-best class up to an explicit stability term (Theorem 4). Empirically, the predicted class matches the empirical winner on all four core benchmarks; TextVQA-OCR provides the deployable Π_3 witness, with a 10.8 joint seed-sd gap over the best lower class.

2 Method

Section 2.1 defines the loss matrix and policy classes; Section 2.2 turns class choice into regime diagnostics and a nested-CV selector.

2.1 Problem setup

We consider an input $x \sim \mathcal{D}$ and a finite action set $\mathcal{A} = \{a_{\text{direct}}, a_{\text{retrieve}}, a_{\text{defer}}, a_{\text{abstain}}\}$. Each action a has correctness $c(x, a) \in \{0, 1\}$, semantic risk $h(x, a) \in [0, 1]$, and operational cost $k(x, a) \geq 0$. The combined task loss is

$$\ell(x, a) = w_c(1 - c(x, a)) + w_h h(x, a) + w_k k(x, a) \in [0, L_{\max}],$$

with non-negative weights (w_c, w_h, w_k) fixed by the deployment. A controller $\pi : \mathcal{X} \rightarrow \mathcal{A}$ has population risk $R(\pi) := \mathbb{E}_{\mathcal{D}}[\ell(x, \pi(x))]$. Setting $w_h = w_k = 0$ recovers raw zero-one accuracy with a_{abstain} costing the same as a wrong direct prediction; classical reject-option theory [Chow, 2003, Franc et al., 2023, Pugnana and Ruggieri, 2023] is the special case in which a_{abstain} is assigned an intermediate cost $c_r \in (0, 1)$ via the semantic-risk channel ($h(x, a_{\text{abstain}}) = c_r, w_h=1$).

Definition 1 (Policy classes). Π_0 is the class of *fixed actions*, $\pi_a(x) \equiv a$. Π_1 is the class of *partition routers*: given a partition $\{G_g\}_{g=1}^K$ and a per-cell action assignment a_g , $\pi(x) = a_g$ when $x \in G_g$. Π_2 contains Π_1 plus *instance-level learned controllers*: measurable maps from per-sample features through a bounded-complexity hypothesis family. Π_3 contains Π_2 plus *prior-gated controllers*: $\pi(x) = \rho(x)$ on inputs where an external prior channel is confident, and $\pi(x) = r(x)$ otherwise, with r drawn from any lower class ($r \in \Pi_0 \cup \Pi_1 \cup \Pi_2$). The deterministic rule ρ uses a channel not visible to r 's feature inputs.

For the set inclusion, view x as the full prediction-time observation; lower classes simply ignore side channels. The four rungs are a constant action, a partition, a per-sample rule, and a side-information gate. If no label-free prediction-time prior is available, the deployable lattice truncates to $\Pi_0 \cup \Pi_1 \cup \Pi_2$.

The classes are nested as sets of functions, so population-optimal risk is monotone: $R(\pi_0^*) \geq R(\pi_1^*) \geq R(\pi_2^*) \geq R(\pi_3^*)$. Estimation complexity goes the other way, and the question is which m minimizes the *expected* risk $\mathbb{E}_S[R(\widehat{\pi}_m(S))]$ at finite n , and whether the answer can be identified from data.

2.2 Finite-sample selection among policy classes

We isolate three bottlenecks: residual mass, Π_2 sample size, and Π_1 partition geometry. Three theorems characterize them, one lemma and one lower bound support the Π_2 analysis, and a final theorem bounds held-out class selection. Throughout, let $a^* := \arg \min_{a \in \mathcal{A}} \mathbb{E}[\ell(x, a)]$ denote the best fixed action and $R := \{x : \exists a, \ell(x, a) < \ell(x, a^*)\}$ the residual set.

We first bound how much any adaptive controller can improve over the best fixed action. If only a small fraction of inputs admit a better action, then the total gain is limited by that fraction times the largest possible per-input improvement.

Theorem 1 (Residual bound). *For any controller $\pi : \mathcal{X} \rightarrow \mathcal{A}$,*

$$\mathbb{E}[\ell(x, a^*) - \ell(x, \pi(x))] \leq \mathbb{P}(R) \cdot \sup_{x \in R, a \in \mathcal{A}} (\ell(x, a^*) - \ell(x, a)).$$

The proof (Appendix B) is a one-line conditioning argument. We next analyze a canonical selective subproblem inside Π_2 only to derive the finite-sample threshold; the evaluated Π_2 families in Section 3 remain multi-action.

A score f induces a rejector π_q : it plays a_{direct} on the top $1-q$ fraction of inputs, ranked by f , and a fallback action on the bottom q . Let L_r, L_w, L_a be the expected losses of a_{direct} on correct inputs, a_{direct} on wrong inputs, and the fallback. Define

$$\alpha_{\min} := \frac{L_a - L_r}{L_w - L_r}, \quad \beta := \alpha_{\text{emp}} - \alpha_{\min},$$

where $\alpha(f)$ is the AUC of f against direct correctness and $\alpha_{\text{emp}} = \sup_f \alpha(f)$ is the AUC ceiling on the feature class. Thus α_{\min} is the break-even AUC for routing the bottom- q to a fallback, and $\beta = \alpha - \alpha_{\min}$ is the margin above break-even.

The asymptotic improvement condition is classical [Chow, 2003, Franc et al., 2023, Pugnana and Ruggieri, 2023]: under the local tail-margin convention introduced in Lemma 1, π_q improves on a_{direct} asymptotically when $\beta > 0$, with reduction of order $q^* \beta (L_w - L_r)$ at optimal q^* (the exact iff condition is on $\mu_w(q) - \alpha_{\min}$, for which β is the AUC-level scalar proxy).

Lemma 1 (Asymptotic signal condition, after [Chow, 2003, Franc et al., 2023]). *The exact improvement condition is on the bottom- q tail precision: π_q improves on a_{direct} asymptotically iff $\mu_w(q) > \alpha_{\min}$ for some q . Suppose $\mu_w(q) - \alpha_{\min}$ shares sign with the AUC margin $\beta = \alpha_{\text{emp}} - \alpha_{\min}$ at the operating q . We use this structural condition throughout as the local tail-margin convention. Under this convention, β is a sufficient scalar proxy: $\beta \leq 0$ rules out asymptotic improvement, and $\beta > 0$ admits scale $q^* \beta (L_w - L_r)$ at optimal coverage q^* .*

The new finite-sample result quantifies how large n must be for the population gain to be visible above estimator variance.

Theorem 2 (Bernstein-tight viability threshold). *Let $\ell \in [0, L_{\max}]$, $\alpha \geq 1/2$, and $\beta = \alpha - \alpha_{\min} > 0$. Assume the local tail-margin condition $\mu_w(q) - \alpha_{\min} \geq \beta$, where $\mu_w(q) := \mathbb{P}(c_{\text{direct}}=0 \mid f(x) \in \text{bottom-}q)$. Then to leading order in n ,*

$$n \geq n_{\min}(\alpha, \beta, q, \delta) := \frac{2\alpha(1-\alpha) \log(2/\delta)}{q\beta^2} \quad (1)$$

is sufficient for the empirical CV loss difference $\widehat{\Delta}(q)$ to have the same sign as the population loss difference with probability at least $1 - \delta$. When n is materially below (1), the bound no longer certifies sign correctness; we call this regime variance-bounded.

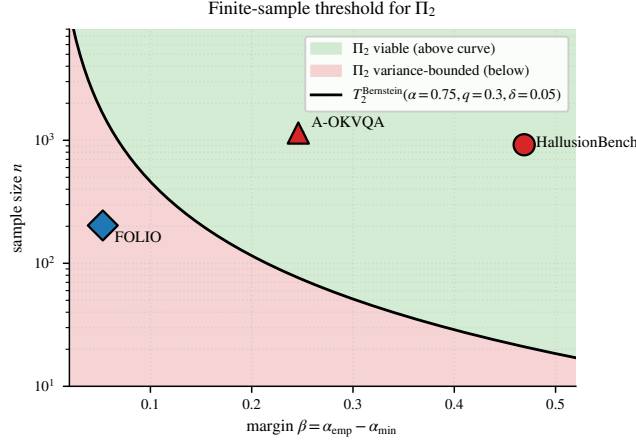


Figure 2: The viability threshold from (1) at $\alpha=0.75, q=0.3, \delta=0.05$. Green: Π_2 -viable. Red: variance-bounded. FOLIO is the one core benchmark far below the Bernstein threshold ($n=203$ vs. $n_{\min}=1898$) and lands deep in the variance-bounded region; its best empirical Π_2 controller slightly increases loss relative to Π_0 (+0.003), consistent with the uncertified-sign regime of Corollary 1 (ii). HallusionBench ($n=920 \gg n_{\min}=23$) and A-OKVQA ($n=1145 \gg n_{\min}=45$) sit comfortably above their respective thresholds. SMS-Spam is governed instead by the residual bound of Theorem 1: its $\beta \leq 0$ violates the positive-margin condition of Theorem 2, so it lies outside the theorem’s viability-threshold regime.

The threshold is computable from $(\alpha, \beta, q, \delta)$ alone (Figure 2). Theorem 2 is the finite-sample counterpart of Jitkrittum et al. [2023]: even with positive asymptotic margin, the sign of a controller’s empirical gain can be uncertified when n is too small. The proof (Appendix B.3) applies Bernstein’s inequality to the bottom- q precision estimator. The next proposition shows that the same dependence on α, β, q , and δ is necessary up to constants.

Proposition 1 (Information-theoretic lower bound). *In the setting of Theorem 2, suppose the bottom- q decision reduces locally to testing $H_0 : \mu_w = \alpha_{\min}$ against $H_1 : \mu_w = \alpha_{\min} + \beta$, with $0 < \beta \leq \frac{1}{2} \min\{\alpha_{\min}, 1 - \alpha_{\min}\}$. Any test that determines the sign of the population loss difference $\Delta(q)$ with both type-I and type-II error at most $\delta \in (0, \frac{1}{8})$ from n i.i.d. samples must satisfy*

$$n \geq \frac{c \alpha (1-\alpha) \log(1/\delta)}{q \beta^2} \quad (2)$$

for a universal constant $c > 0$. Since the sufficient condition (1) has the same functional form $n_{\min} = 2\alpha(1-\alpha) \log(2/\delta)/(q\beta^2)$, the viability threshold has the optimal high-confidence order under this reduction: $n_{\min} \asymp \alpha(1-\alpha) \log(1/\delta)/(q\beta^2)$, up to universal constants and the local replacement of α_{\min} by $\alpha = \alpha_{\min} + \beta$.

The proof (Appendix B.4) is Bretagnolle–Huber on the local Bernoulli alternative [Tsybakov, 2009]. Thus, under the local testing reduction, the threshold is order-tight.

A coarser controller can win where Π_2 is variance-bounded, not because it is more powerful, but because it asks less of the data: a partition router only needs each group to have a clear best action, not a precise per-sample score, so its sample complexity depends on cluster mass and gap rather than on the per-sample margin that controls Π_2 . Let $\mathcal{G} = \{G_g\}_{g=1}^K$ be a measurable partition with $p_g := \mathbb{P}(x \in G_g)$, cell-best actions $a_g^* := \arg \min_a \mathbb{E}[\ell(x, a) \mid x \in G_g]$, and discriminability gaps $\gamma_g := \mathbb{E}[\ell(x, a^*) - \ell(x, a_g^*) \mid x \in G_g] \geq 0$.

Theorem 3 (Distribution-dependent partition lower bound). *For any measurable partition \mathcal{G} with cluster probabilities p_g and discriminability gaps γ_g ,*

$$\Delta_{\text{partition}}(\mathcal{G}) = \sum_{g=1}^K p_g \gamma_g \geq \max_g p_g \gamma_g. \quad (3)$$

Moreover, let σ^2 be an upper bound on the per-action conditional loss variance on any cell. Under Bernstein concentration on each cell, the empirical Π_1 estimator with κ -fold CV on n samples achieves cell-loss no worse than the global baseline a^* on cluster g (i.e. secures the corresponding $p_g\gamma_g$ contribution to (3)) with probability at least $1 - \delta$ whenever $n \geq \frac{\kappa}{\kappa-1} \max\{8 \log(2/\delta)/p_g, (16\sigma^2 + (8/3)L_{\max}\gamma_g) \log(4|\mathcal{A}|/\delta)/(p_g\gamma_g^2)\}$, where the first term is a Chernoff occupancy floor and the second the Bernstein concentration term. The sample complexity depends on p_g and γ_g but not on the instance-level margin β .

The sample complexity scales with p_g and γ_g , not with the per-sample margin β that controls Π_2 , so a partition router can succeed precisely where an instance-level controller is variance-bounded. The $\max_g p_g\gamma_g$ form is also diagnostic: when the empirical reduction is close to it, the partition win is essentially a one-cluster phenomenon. Proof is in Appendix B; the bound is agnostic, and an adaptive partition such as KMeans can be tighter, which we treat as an empirical observation (Appendix D.2).

For comparing supportable adaptive classes, write

$$C_{\Pi_1}(\mathcal{G}) := \sum_g p_g\gamma_g, \quad C_{\Pi_1} := \max_{\mathcal{G} \in \mathfrak{G}} C_{\Pi_1}(\mathcal{G}),$$

for a candidate partition family \mathfrak{G} , and

$$C_{\Pi_2} := q^* \beta (L_w - L_r)$$

for the AUC-level Π_2 ceiling. The residual product, the Π_2 viability test ($n \geq n_{\min}$), and the two ceilings C_{Π_1}, C_{Π_2} give the regime decomposition:

Corollary 1 (Regime decomposition). *For (\mathcal{D}, n) , (i) every adaptive class is capped by the residual product in Theorem 1; when this product is small, no adaptive class can improve by more than residual scale. (ii) If $\beta > 0$ but $n < n_{\min}$, Π_2 's sign is uncertified, while Π_1 can strictly improve on Π_0 whenever some candidate partition has $C_{\Pi_1}(\mathcal{G}) > 0$. (iii) If $n \geq n_{\min}$, the population-optimal winner between Π_1 and Π_2 is determined by comparison between the ceilings C_{Π_1} and C_{Π_2} ; the empirical winner additionally depends on how tightly the deployed candidate families realize each ceiling at finite n .*

When benchmarks fall into different cases, no single controller family is uniformly optimal. Corollary 1 is the regime diagnostic; Section 3 uses strict nested CV over candidate classes, and Theorem 4 bounds the held-out selection cost. The bound is stated for the inner-CV estimand because validation-based selection can itself overfit [Cawley and Talbot, 2010].

Theorem 4 (Held-out selection bound). *Let $\mathcal{M} \subseteq \{0, 1, 2, 3\}$ be the candidate classes ($|\mathcal{M}| = 3$ when no deployable external channel is available). Let $\widehat{R}_{\text{CV}}(m)$ be the inner κ -fold CV estimate and $\bar{R}_\kappa(m)$ the expected risk of an inner-trained estimator. With $\widehat{m} := \arg \min_{m \in \mathcal{M}} \widehat{R}_{\text{CV}}(m)$ and $\ell \in [0, L_{\max}]$,*

$$\mathbb{E}[\bar{R}_\kappa(\widehat{m})] \leq \min_{m \in \mathcal{M}} \bar{R}_\kappa(m) + 4L_{\max} \sqrt{\log(2|\mathcal{M}|)/n_{\text{in}}}, \quad (4)$$

where $n_{\text{in}} = n_{\text{out}}/\kappa$. *If each estimator is $\varepsilon_{\text{stab}}$ -stable when refit from inner-train to outer-train, the bound transfers to the refit estimator with an added $2\varepsilon_{\text{stab}}$ term.*

The proof (Appendix B.6) is Hoeffding plus a union bound over \mathcal{M} . The \min_m on the right absorbs the class-specific estimation errors controlled by Theorems 2–3: zero for $m=0$, partition complexity for $m=1$, and the Bernstein threshold for $m=2$.

3 Experiments

Experimental protocol and data. We instantiate the lattice as a controller pool under strict nested 5-fold-by-5-seed CV: family selection on outer-train via inner CV, refit on outer-train, single evaluation on outer-test. The pool keeps Π_0 at always-direct and a fair-fixed CV variant; Π_1 uses KMeans partition routers ($K \in \{4, 5, 6, 8\}$); Π_2 uses HGBC ($\text{md} \in \{3, 4\}$) and a calibrated logistic plug-in ($C=0.3$). Hyperparameters are fixed in advance, not tuned per benchmark; a structurally different CART partition variant of Π_1 is reported as an ablation (Appendix F.2). Reported \pm values are 5-seed standard deviations; gaps in seed-sd units reflect algorithmic stability rather than dataset-resampling

Benchmark	Π_0 best↓	Π_1 best↓	Π_2 best↓	predicted
SMS-Spam ($n=1114$)	0.0590 ± 0.0000	0.0590 ± 0.0000 †	0.0591 ± 0.0000	Π_0
HallusionBench ($n=920$)	1.0000 ± 0.0000	0.9093 ± 0.0025	0.8970 ± 0.0039	Π_2
A-OKVQA ($n=1145$)	0.4138 ± 0.0000	0.3902 ± 0.0085	0.3805 ± 0.0032	Π_2
FOLIO ($n=203$)	0.7520 ± 0.0000	0.7195 ± 0.0073	0.7546 ± 0.0086	Π_1

Table 1: Strict nested 5-fold-by-5-seed CV per-class loss on the four core benchmarks (lower is better; values are mean \pm seed-sd, fixed policies have zero seed variance). Bold marks the empirical winner within $\Pi_0 \cup \Pi_1 \cup \Pi_2$; the rightmost column gives the regime-theoretic predicted winner from Theorem 2 and Corollary 1 (full predictions with diagnostics in Table 2). †: on SMS-Spam, Π_1 collapses to a_{direct} under CV, so $\Pi_1 = \Pi_0$ numerically; Π_0 is the strict winner because Π_2 is +0.0002 worse. Per-benchmark mechanism (including `fair_fixed_train` on HallusionBench and the uncertified Π_2 outcome on FOLIO) is unpacked in the body.

error. Implementation details are in Appendices C.3–C.4; cost-sensitive L2D adaptations [Mozannar and Sontag, 2020, Narasimhan et al., 2022] are reported in Appendix F.1.

We report results on four full-corpus benchmarks; each regime tag follows from $(\alpha, \beta, n, \{p_g \gamma_g\})$ computed on the held-out split, independent of any per-class CV outcome. The benchmarks: SMS-Spam [Almeida et al., 2011] (saturated text, residual-bounded), HallusionBench [Guan et al., 2024] (visual hallucination, large- β), A-OKVQA [Schwenk et al., 2022] (near-tie Π_1/Π_2), and FOLIO [Han et al., 2024] (small β and $n < n_{\min}^{\text{Bern}}$, variance-bounded). On HallusionBench/A-OKVQA, a_{direct} and a_{retrieve} are produced by Qwen2.5-VL-3B-Instruct (a_{retrieve} : 2-turn grounded-context pass) and a_{defer} by Qwen2.5-VL-7B-Instruct ($c_{\text{defer}}/c_{\text{direct}}=2.3$); FOLIO uses the same backbones in text-only mode. Per-action risk $h(x, a) \in \{0, 0.5, 1\}$ on HallusionBench/A-OKVQA comes from an InternVL2.5-8B [Chen et al., 2024b] judge *drawn from a different VLM family than the upstream Qwen2.5-VL policies*, so the judge does not score outputs from its own family; FOLIO uses a rule-based risk channel ($h=0.5$ on wrong, 0 on correct), and SMS-Spam uses canonical-cost weighting without a judge. Canonical weights $(w_c, w_h, w_k) = (1, 1, 0.05)$; weight robustness in Appendix F.2.

Controllers consume a scalar feature block of 41 dims on HallusionBench, 39 dims on A-OKVQA, 12 dims on FOLIO/SMS-Spam, all derived from upstream Qwen2.5-VL outputs at prediction time. The InternVL2.5-8B judge is used only to label semantic risk in the loss matrix and is never exposed to the controller (Appendices D, C.2). None of the four core benchmarks supplies a label-free prediction-time prior channel, so the deployable lattice truncates to $\Pi_0 \cup \Pi_1 \cup \Pi_2$; we use TextVQA [Singh et al., 2019] for a separate Π_3 test.

Each benchmark uses its full native held-out split (n values in Table 1; HallusionBench drops 31 of 951 rows with empty Qwen-VL-3B commitments), spanning four $(\alpha, \beta, n, \{p_g \gamma_g\})$ regimes; the controlled n -sweep is deferred to Appendix E.1.

Main result. Table 1 and Figure 3 give deployable per-class winners; the pattern aligns with Corollary 1. *SMS-Spam* (residual-bounded, $\mathbb{P}(R)=0.009$): every Π_1 family collapses to direct in CV and the best Π_2 family is +0.0002 worse, so Π_0 strictly wins (Appendix D.1). *HallusionBench* (Bernstein-viable, $n=920 \gg n_{\min}^{\text{Bern}}=23$): Π_2 (HGBC-md3, -0.103 , 26 seed-sd) edges Π_1 (KMeans- $K=8$, -0.091) by ≈ 3 seed-sd; inner-CV picks Π_2 on 20/25 outer-folds (Appendix F.3); the instance ceiling exceeds the partition ceiling (Cor 1 (iii)). *A-OKVQA* (Π_1/Π_2 boundary): Π_2 (Selective- $C=0.3$, -0.033) edges Π_1 (KMeans- $K=4$, -0.024) by ≈ 1 seed-sd; inner-CV splits $\Pi_1:\Pi_2$ as 10:15 over 25 folds. *FOLIO* (variance-bounded, $n=203 \ll n_{\min}^{\text{Bern}}=1898$; Cor 1 (ii)): Π_1 (KMeans- $K=6$, -0.033 , 4.5 seed-sd) wins; the best Π_2 controller slightly increases loss relative to Π_0 (+0.0027), and cost-sensitive L2D adaptations [Mozannar and Sontag, 2020, Narasimhan et al., 2022] (both Π_2 -class) reach 0.7478 and 0.7705, trailing our Π_1 by 0.028/0.051 (Appendix F.1). The A-OKVQA Π_3 rationale experiment is excluded from the deployable comparison because rationales are answer-derived (Appendix D.4).

Theory-to-benchmark match. Table 2 instantiates the diagnostics behind Figure 3. FOLIO lies far below the Bernstein threshold ($n\beta^2=0.57$, $n_{\min}=1898$), where Π_2 ’s sign is uncertified (Cor 1 (ii)) and the supportable adaptive winner is Π_1 . HallusionBench resolves via $C_{\Pi_2} > C_{\Pi_1}$ (Cor 1 (iii), Π_2 winner); A-OKVQA is a Π_1/Π_2 boundary case, reflected in the 10:15 inner-CV class split

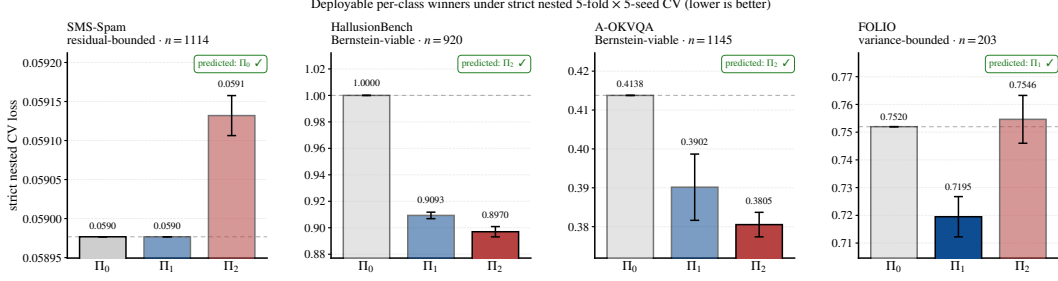


Figure 3: Deployable per-class winners under strict nested 5-fold-by-5-seed CV on the four core benchmarks (lower is better). Error bars are multi-seed standard deviations. Gold outlines mark the deployable per-benchmark winner within $\Pi_0 \cup \Pi_1 \cup \Pi_2$. The winning class changes across benchmarks in the pattern indicated by the regime diagnostics: Π_0 on SMS-Spam (residual-bounded), Π_2 on HallusionBench and A-OKVQA (Bernstein-viable, with A-OKVQA near the Π_1/Π_2 boundary), and Π_1 on FOLIO (variance-bounded; Π_2 's sign uncertified). The non-deployable A-OKVQA Π_3 gold-rationale oracle is reported separately in Table 4.

Benchmark	n	α_{emp}	β	$n\beta^2$	n_{\min}^{Bern}	C_{Π_1}	C_{Π_2}	predicted class
SMS-Spam	1114	0.991	$\leq 0^\dagger$	—	—	0.000	—	Π_0 (residual-bounded; Thm 1)
HallusionBench	920	0.722	0.469	202.4	23	0.10	0.15	Π_2 (high-signal, $n \gg n_{\min}$; Thm 2)
A-OKVQA	1145	0.874	0.246	69.3	45	0.039	0.094	Π_2 (high-signal, Π_1/Π_2 boundary)
FOLIO	203	0.687	0.053	0.57	1898	0.065	0.024 ‡	Π_1 ($n < n_{\min}$, Π_2 uncertified; Cor 1 (ii))

Table 2: Theory-instantiated quantities from Theorem 2 and Corollary 1. n_{\min}^{Bern} is computed from the leading-order formula $\lceil 2\alpha(1-\alpha) \log(2/\delta)/(q\beta^2) \rceil$ at $\delta=0.05$, $q=0.3$, using the cross-validated AUC margin as the local tail-margin proxy. $C_{\Pi_1} = \max_{g \in \mathcal{G}} \sum_g p_g \gamma_g$ over the candidate KMeans family; $C_{\Pi_2} = q^* \beta (L_w - L_r)$. Bold marks the diagnostic favoring the predicted adaptive class: for HallusionBench and A-OKVQA both classes are supportable and the larger ceiling indicates the Cor 1 (iii) winner; for FOLIO Π_2 is uncertified ($n < n_{\min}^{\text{Bern}}$, Cor 1 (ii)) so C_{Π_1} is bolded as the supportable winner. † SMS-Spam: $\beta \leq 0$, Lemma 1 rules out an instance-level rejector; $\mathbb{P}(R)=0.009$, oracle Π_2 gain = 0.003. ‡ FOLIO: C_{Π_2} is the asymptotic ceiling but Π_2 's sign is uncertified at $n=203 < n_{\min}^{\text{Bern}}$, so the empirical winner falls to Π_1 . Diagnostics are reported post-hoc on outer-test concatenations; the strict-CV selection rule uses only inner-fold quantities (Theorem 4; auto-pick analysis in Appendix F.3).

(Appendix F.3); SMS-Spam has $\beta \leq 0$ and is governed by the residual bound (Thm 1; Appendix D.1). The classification is unchanged at $q \in \{0.2, 0.3, 0.4\}$.

TextVQA-OCR: deployable Π_3 . The four core benchmarks above span the deployable $\Pi_0 \cup \Pi_1 \cup \Pi_2$ lattice; we now turn to the top rung. Π_3 requires a label-free prediction-time prior channel, and TextVQA is the one benchmark in our pool that supplies one: OCR tokens are image-derived and observable before answering. We freeze two upstream actions on the official training split (a question/image-class direct predictor and an OCR-copy predictor), then route on the official validation split ($n=5000$) under strict 5-fold-by-5-seed CV. Lower rungs see only scalar non-OCR features (the Π_1 pool here also includes a CART variant over that block). Π_3 alone gates on OCR-prior confidence and sends the rest to a learned fallback. Loss is 1-soft-VQA accuracy.

The fixed OCR action reaches 15.4% soft accuracy versus direct's 8.4%, so the benchmark contains usable side information that the scalar feature block cannot recover. Π_2 on non-OCR features is actually *worse* than the fixed OCR action (0.8595 vs. 0.8463): an information-design issue, not a Bernstein-threshold failure at $n=5000$. Π_3 resolves this by gating high-confidence OCR cases on the prior and sending the rest to a learned fallback, reducing loss by 0.0233 over the best lower class. The synthetic in Appendix E.3 constructs the prior independent of X , confirming Π_2 's lack of access cannot be rescued by additional samples.

Additional checks. Appendix analyses corroborate the regime map: a bottom- q precision-estimator cross-threshold synthetic for Theorem 2 that sweeps n across $n_{\min}(\beta)$ and recovers the predicted

TextVQA-OCR validation ($n=5000$)	best family	answer loss	Δ vs Π_3
Π_0	always_ocr	0.8463 ± 0.0000	+0.0251
Π_1	CART-d4	0.8445 ± 0.0006	+0.0233
Π_2	logistic $C=0.3$	0.8595 ± 0.0021	+0.0383
Π_3	OCR gate + fallback	0.8212 ± 0.0021	0

Table 3: Deployable Π_3 on TextVQA-OCR. Lower rungs see only scalar non-OCR features; Π_3 alone gates on OCR-prior confidence. Π_2 underperforms Π_0 because non-OCR features cannot recover OCR-side information (information-design issue, not a Bernstein-threshold failure: $n=5000$ is well above n_{\min}). Π_3 ’s 0.0233 gap over best-lower Π_1 is 10.8 joint seed-sd ($\sigma_j=0.00217$).

sign-correctness transition (Appendix E.1); the Π_1/Π_2 and Π_3 synthetics (Appendices E.2, E.3); HallusionBench cluster anatomy with $\sum_g p_g \gamma_g=0.047$ at $K=4$ saturating the empirical KM- $K=4$ loss reduction 0.048 ± 0.005 (Appendix D.2); CART and loss-weight ablations (Appendix F.2).

4 Related Work

Selective classification, learning to defer, and cascade routing. A long line of work fixes a single controller family and refines the score, surrogate, or calibrator within it—from classical reject-option theory [Chow, 2003, El-Yaniv et al., 2010, Geifman and El-Yaniv, 2017, Franc et al., 2023, Pugnana and Ruggieri, 2023, Traub et al., 2024] to cost-sensitive deferral [Mozannar and Sontag, 2020, Narasimhan et al., 2022, Verma et al., 2023, Mao et al., 2023]. Cascade routing [Chen et al., 2023, Ding et al., 2024, Ong et al., 2024, Chen et al., 2024a, Dekoninck et al., 2024] extends this to a cost-ordered model sequence but keeps the family fixed; Goren et al. [2024] nest abstention in the *output* space rather than in the controller space we study. Conformal prediction [Angelopoulos and Bates, 2023, Bates et al., 2021] calibrates a threshold inside a fixed selective family. We instead ask which family the available n can support: our viability threshold is the finite-sample counterpart of Jitkrittum et al. [2023]’s sufficient-statistic characterization, and our held-out selection bound (Theorem 4) adapts classical nested-CV concerns [Cawley and Talbot, 2010] from within-family hyperparameter selection to controller-class selection.

Gate-and-residual hybrids and hallucination impossibility. Combining a deterministic gate with a learned fallback recurs across selective generation [Chen et al., 2023, Dekoninck et al., 2024, Jeong et al., 2024, Asai et al., 2023]. Π_3 singles out the subclass with a *deterministic* rule on a channel disjoint from the fallback’s feature block, and gives the regime-theoretic conditions under which this restriction strictly dominates a learned Π_2 —and when the Π_1 fallback wins instead. The lattice motivation is sharper where instance-level signal is structurally limited: Kalai and Vempala [2024] and Karbasi et al. [2025] prove lower bounds on hallucination detection from same-information-source signals; Theorem 2 provides a finite-sample viability threshold in the same spirit, and Theorem 3 identifies when Π_1 can recover loss in this regime. Mitigation approaches in this literature change decoding [Leng et al., 2024], the feature space [Farquhar et al., 2024], or the action set [Srinivasan et al., 2024, Whitehead et al., 2022].

5 Discussion

Residual mass, sample size, and partition geometry are three genuinely distinct bottlenecks, and which one binds determines which class wins. Each check is computable from a held-out probe and maps to one of the theorems, and the same selection rule places Π_0 , Π_1 , Π_2 , and Π_3 in their predicted regimes across superficially similar benchmarks, arguing that family choice, not within-family refinement, is where most of the loss comes from.

Two boundary conditions sharpen the claims: Π_3 requires a label-free prior, and Theorems 1–4 depend only on $(\alpha, \beta, n, \mathbb{P}(R), \{p_g \gamma_g\})$, so changing the policy pair or judge moves the diagnostics but not the rule. The bottlenecks bind differently across benchmarks (Theorem 3 tight on HallusionBench, uncertified Π_2 on FOLIO, 0.0233-loss Π_3 gap on TextVQA-OCR); reliable deferred deployment is about matching class to data.

References

- Tiago A Almeida, José María G Hidalgo, and Akebo Yamakami. Contributions to the study of sms spam filtering: new collection and results. In *Proceedings of the 11th ACM symposium on Document engineering*, pages 259–262, 2011.
- Anastasios N Angelopoulos and Stephen Bates. Conformal prediction: A gentle introduction. *Foundations and Trends in Machine Learning*, 16(4):494–591, 2023.
- Akari Asai, Zeqiu Wu, Yizhong Wang, Avirup Sil, and Hannaneh Hajishirzi. Self-rag: Learning to retrieve, generate, and critique through self-reflection. In *The Twelfth International Conference on Learning Representations*, 2023.
- Stephen Bates, Anastasios Angelopoulos, Lihua Lei, Jitendra Malik, and Michael Jordan. Distribution-free, risk-controlling prediction sets. *Journal of the ACM (JACM)*, 68(6):1–34, 2021.
- Stéphane Boucheron, Gábor Lugosi, and Pascal Massart. *Concentration Inequalities: A Nonasymptotic Theory of Independence*. Oxford University Press, 02 2013. ISBN 9780199535255. doi: 10.1093/acprof:oso/9780199535255.001.0001. URL <https://doi.org/10.1093/acprof:oso/9780199535255.001.0001>.
- Gavin C Cawley and Nicola LC Talbot. On over-fitting in model selection and subsequent selection bias in performance evaluation. *The Journal of Machine Learning Research*, 11:2079–2107, 2010.
- Lingjiao Chen, Matei Zaharia, and James Zou. Frugalgpt: How to use large language models while reducing cost and improving performance. *arXiv preprint arXiv:2305.05176*, 2023.
- Shuhao Chen, Weisen Jiang, Baijiong Lin, James Kwok, and Yu Zhang. Routerdc: Query-based router by dual contrastive learning for assembling large language models. *Advances in Neural Information Processing Systems*, 37:66305–66328, 2024a.
- Zhe Chen, Jiannan Wu, Wenhai Wang, Weijie Su, Guo Chen, Sen Xing, Muyan Zhong, Qinglong Zhang, Xizhou Zhu, Lewei Lu, et al. Internvl: Scaling up vision foundation models and aligning for generic visual-linguistic tasks. In *Proceedings of the IEEE/CVF conference on computer vision and pattern recognition*, pages 24185–24198, 2024b.
- C Chow. On optimum recognition error and reject tradeoff. *IEEE Transactions on information theory*, 16(1):41–46, 2003.
- Jasper Dekoninck, Maximilian Baader, and Martin Vechev. A unified approach to routing and cascading for llms. *arXiv preprint arXiv:2410.10347*, 2024.
- Dujian Ding, Ankur Mallick, Chi Wang, Robert Sim, Subhabrata Mukherjee, Victor Ruhle, Laks VS Lakshmanan, and Ahmed Hassan Awadallah. Hybrid llm: Cost-efficient and quality-aware query routing. *arXiv preprint arXiv:2404.14618*, 2024.
- Chris Drummond and Robert C Holte. Cost curves: An improved method for visualizing classifier performance. *Machine learning*, 65(1):95–130, 2006.
- Ran El-Yaniv et al. On the foundations of noise-free selective classification. *Journal of Machine Learning Research*, 11(5), 2010.
- Sebastian Farquhar, Jannik Kossen, Lorenz Kuhn, and Yarin Gal. Detecting hallucinations in large language models using semantic entropy. *Nature*, 630(8017):625–630, 2024.
- Vojtech Franc, Daniel Prusa, and Vaclav Voracek. Optimal strategies for reject option classifiers. *Journal of Machine Learning Research*, 24(11):1–49, 2023.
- Yonatan Geifman and Ran El-Yaniv. Selective classification for deep neural networks. *Advances in neural information processing systems*, 30, 2017.
- Shani Goren, Ido Galil, and Ran El-Yaniv. Hierarchical selective classification. *Advances in Neural Information Processing Systems*, 37:111047–111073, 2024.

- Tianrui Guan, Fuxiao Liu, Xiyang Wu, Ruiqi Xian, Zongxia Li, Xiaoyu Liu, Xijun Wang, Lichang Chen, Furong Huang, Yaser Yacoob, et al. Hallusionbench: an advanced diagnostic suite for entangled language hallucination and visual illusion in large vision-language models. In *Proceedings of the IEEE/CVF conference on computer vision and pattern recognition*, pages 14375–14385, 2024.
- Simeng Han, Hailey Schoelkopf, Yilun Zhao, Zhenting Qi, Martin Riddell, Wenfei Zhou, James Coady, David Peng, Yujie Qiao, Luke Benson, et al. Folio: Natural language reasoning with first-order logic. In *Proceedings of the 2024 Conference on Empirical Methods in Natural Language Processing*, pages 22017–22031, 2024.
- Gautier Izacard, Patrick Lewis, Maria Lomeli, Lucas Hosseini, Fabio Petroni, Timo Schick, Jane Dwivedi-Yu, Armand Joulin, Sebastian Riedel, and Edouard Grave. Atlas: Few-shot learning with retrieval augmented language models. *Journal of Machine Learning Research*, 24(251):1–43, 2023.
- Soyeong Jeong, Jinheon Baek, Sukmin Cho, Sung Ju Hwang, and Jong C Park. Adaptive-rag: Learning to adapt retrieval-augmented large language models through question complexity. In *Proceedings of the 2024 Conference of the North American Chapter of the Association for Computational Linguistics: Human Language Technologies (Volume 1: Long Papers)*, pages 7036–7050, 2024.
- Wittawat Jitkrittum, Neha Gupta, Aditya Krishna Menon, Harikrishna Narasimhan, Ankit Singh Rawat, and Sanjiv Kumar. When does confidence-based cascade deferral suffice?, 2024. [URL https://arxiv.org/abs/2307.02764](https://arxiv.org/abs/2307.02764), 2023.
- Adam Tauman Kalai and Santosh S Vempala. Calibrated language models must hallucinate. In *Proceedings of the 56th Annual ACM Symposium on Theory of Computing*, pages 160–171, 2024.
- Amin Karbasi, Omar Montasser, John Sous, and Grigoris Velegkas. (im) possibility of automated hallucination detection in large language models. *arXiv preprint arXiv:2504.17004*, 2025.
- Vladimir Karpukhin, Barlas Oguz, Sewon Min, Patrick Lewis, Ledell Wu, Sergey Edunov, Danqi Chen, and Wen-tau Yih. Dense passage retrieval for open-domain question answering. In *Proceedings of the 2020 conference on empirical methods in natural language processing (EMNLP)*, pages 6769–6781, 2020.
- Sicong Leng, Hang Zhang, Guanzheng Chen, Xin Li, Shijian Lu, Chunyan Miao, and Lidong Bing. Mitigating object hallucinations in large vision-language models through visual contrastive decoding. In *Proceedings of the IEEE/CVF Conference on Computer Vision and Pattern Recognition*, pages 13872–13882, 2024.
- Patrick Lewis, Ethan Perez, Aleksandra Piktus, Fabio Petroni, Vladimir Karpukhin, Naman Goyal, Heinrich Küttler, Mike Lewis, Wen-tau Yih, Tim Rocktäschel, et al. Retrieval-augmented generation for knowledge-intensive nlp tasks. *Advances in neural information processing systems*, 33: 9459–9474, 2020.
- Anqi Mao, Christopher Mohri, Mehryar Mohri, and Yutao Zhong. Two-stage learning to defer with multiple experts. *Advances in neural information processing systems*, 36:3578–3606, 2023.
- Hussein Mozannar and David Sontag. Consistent estimators for learning to defer to an expert. In *International conference on machine learning*, pages 7076–7087. PMLR, 2020.
- Harikrishna Narasimhan, Wittawat Jitkrittum, Aditya K Menon, Ankit Rawat, and Sanjiv Kumar. Post-hoc estimators for learning to defer to an expert. *Advances in Neural Information Processing Systems*, 35:29292–29304, 2022.
- Isaac Ong, Amjad Almahairi, Vincent Wu, Wei-Lin Chiang, Tianhao Wu, Joseph E Gonzalez, M Waleed Kadous, and Ion Stoica. Routellm: Learning to route llms with preference data. *arXiv preprint arXiv:2406.18665*, 2024.
- Andrea Pugnana and Salvatore Ruggieri. Auc-based selective classification. In *International conference on artificial intelligence and statistics*, pages 2494–2514. PMLR, 2023.

- Dustin Schwenk, Apoorv Khandelwal, Christopher Clark, Kenneth Marino, and Roozbeh Mottaghi. A-okvqa: A benchmark for visual question answering using world knowledge. In *European conference on computer vision*, pages 146–162. Springer, 2022.
- Amanpreet Singh, Vivek Natarajan, Meet Shah, Yu Jiang, Xinlei Chen, Dhruv Batra, Devi Parikh, and Marcus Rohrbach. Towards vqa models that can read. In *Proceedings of the IEEE/CVF conference on computer vision and pattern recognition*, pages 8317–8326, 2019.
- Tejas Srinivasan, Jack Hessel, Tanmay Gupta, Bill Yuchen Lin, Yejin Choi, Jesse Thomason, and Khyathi Chandu. Selective “selective prediction”: Reducing unnecessary abstention in vision-language reasoning. In *Findings of the Association for Computational Linguistics: ACL 2024*, pages 12935–12948, 2024.
- Jeremias Traub, Till J Bungert, Carsten T Lüth, Michael Baumgartner, Klaus H Maier-Hein, Lena Maier-Hein, and Paul F Jäger. Overcoming common flaws in the evaluation of selective classification systems. *Advances in Neural Information Processing Systems*, 37:2323–2347, 2024.
- Alexandre B. Tsybakov. *Introduction to Nonparametric Estimation*. Springer, 2009.
- Rajeev Verma, Daniel Barrejón, and Eric Nalisnick. Learning to defer to multiple experts: Consistent surrogate losses, confidence calibration, and conformal ensembles. In *International Conference on Artificial Intelligence and Statistics*, pages 11415–11434. PMLR, 2023.
- Roman Vershynin. *High-dimensional probability: An introduction with applications in data science*, volume 47. Cambridge university press, 2018.
- Spencer Whitehead, Suzanne Petryk, Vedaad Shakib, Joseph Gonzalez, Trevor Darrell, Anna Rohrbach, and Marcus Rohrbach. Reliable visual question answering: Abstain rather than answer incorrectly. In *European Conference on Computer Vision*, pages 148–166. Springer, 2022.

A Limitations

The regime diagnostics are conditional on the chosen action set, loss matrix, feature block, and judge; changing these ingredients can move a benchmark to a different regime, although the same diagnostics can be recomputed. The Bernstein analysis is derived for a selective subproblem and used as a class-level viability proxy for richer multi-action controllers. When the asymptotic ceilings C_{Π_1} and C_{Π_2} are commensurate, the empirical winner can depend on how well the deployed candidate families realize their ceilings; Corollary 1 (iii)’s class prediction is population-optimal but mediated by family capacity at finite n (Appendix E.2). Semantic-risk labels on HallusionBench and A-OKVQA come from a single judge (InternVL2.5-8B) from a different VLM family than the upstream policies; alternative judges or ensembles could shift the loss matrix and therefore the regime tags. The Π_3 rung further requires a label-free prediction-time prior channel, and our empirical coverage is limited to the benchmarks studied here.

B Proofs

B.1 Theorem 1 (residual bound)

Let $g(x) := \ell(x, a^*) - \ell(x, \pi(x))$. On R^c , by the definition of the residual set, $\ell(x, a^*) \leq \ell(x, a)$ for every $a \in \mathcal{A}$, so $g(x) \leq 0$ on R^c . Therefore

$$\mathbb{E}[g(x)] = \mathbb{E}[g(x)\mathbf{1}_R] + \mathbb{E}[g(x)\mathbf{1}_{R^c}] \leq \mathbb{E}[g(x)\mathbf{1}_R] \leq \mathbb{P}(R) \sup_{x \in R, a \in \mathcal{A}} (\ell(x, a^*) - \ell(x, a)),$$

which is the stated bound. \square

B.2 Lemma 1 (asymptotic signal condition)

The Chow-style derivation in [Chow, 2003] and its selective-risk extensions [Franc et al., 2023, Pugnana and Ruggieri, 2023] give that the population loss difference of the rejector at coverage q induced by f , relative to the fixed direct policy, is

$$\Delta L(q) = -q(L_w - L_r)(\mu_w(q) - \alpha_{\min}),$$

where $\mu_w(q)$ is the population precision of the rejected set. Thus the exact improvement condition is $\mu_w(q) > \alpha_{\min}$. The AUC margin $\beta = \alpha_{\text{emp}} - \alpha_{\min}$ used in the main text is a scalar proxy for this working-point margin, not an identity between AUC and tail precision. Under the local tail-margin convention stated before Theorem 2, the certified loss-reduction scale is $q^* \beta (L_w - L_r)$ after optimizing over $q \in (0, 1]$. \square

B.3 Theorem 2 (Bernstein-tight viability threshold)

Let $m := \lfloor nq \rfloor$ and let $\hat{\mu}_w(q)$ be the empirical precision on the m samples with the lowest f -scores. Conditional on f (trained on a held-out split under our nested-CV protocol), the bottom- q labels are independent Bernoulli draws with average success probability $\mu_w(q)$; per-sample probabilities can vary across the bin, but the empirical-mean variance bound $\sigma^2 \leq \mu_w(q)(1 - \mu_w(q))$ holds for the sample mean either way, and is in turn bounded by $\alpha(1 - \alpha)$ for positive-margin rankers with $\alpha \geq 1/2$. The deviation bound below thus controls the precision-proxy loss difference $\hat{\Delta}(q) = -q(L_w - L_r)(\hat{\mu}_w(q) - \alpha_{\min})$ with L_w, L_r treated as published constants; the additional fold-wise variance from estimating L_w, L_r themselves is controlled separately by the action-conditional sample means and is dominated by the Bernoulli term whenever (1) binds.

Bernstein’s inequality [Boucheron et al., 2013, Vershynin, 2018] in deviation form gives, with probability at least $1 - \delta$,

$$|\hat{\mu}_w(q) - \mu_w(q)| \leq \sqrt{\frac{2\sigma^2 \log(2/\delta)}{m}} + \frac{2}{3} \cdot \frac{\log(2/\delta)}{m}.$$

The empirical loss difference is $\hat{\Delta}(q) = -q(L_w - L_r)(\hat{\mu}_w(q) - \alpha_{\min})$, so $|\hat{\Delta}(q) - \Delta(q)| = q(L_w - L_r)|\hat{\mu}_w(q) - \mu_w(q)|$. Substituting the Bernstein deviation and using $m = nq$ together with $\sigma^2 \leq \alpha(1 - \alpha)$, the condition $|\Delta(q)| \geq |\hat{\Delta}(q) - \Delta(q)|$ (which suffices for $\hat{\Delta}(q) < 0$ with probability at least $1 - \delta$) becomes, after cancelling $q(L_w - L_r)$,

$$\beta \geq \sqrt{\frac{2\alpha(1-\alpha) \log(2/\delta)}{nq}} + \frac{2}{3} \cdot \frac{\log(2/\delta)}{nq}.$$

The dominant term on the right is of order $1/\sqrt{n}$ and the sub-leading term is of order $1/n$. Dropping the sub-leading term and squaring the resulting inequality $\beta^2 \geq 2\alpha(1 - \alpha) \log(2/\delta)/(nq)$ gives the leading-order sufficient condition $n \geq 2\alpha(1 - \alpha) \log(2/\delta)/(q\beta^2)$, which is precisely (1). The dropped correction is of lower order in n and does not change the qualitative regime classification (Section 3 reports per-benchmark instantiations). \square

B.4 Proposition 1 (information-theoretic lower bound)

The sign of the loss difference $\Delta(q)$ is determined by whether the bottom- q precision $\mu_w(q)$ exceeds α_{\min} . Any test that determines this sign from n i.i.d. samples must in particular solve the binary hypothesis test $H_0 : \mu_w = \alpha_{\min}$ versus $H_1 : \mu_w = \alpha_{\min} + \beta$ using the $m = \lfloor nq \rfloor$ Bernoulli observations (wrong/right labels) in the rejected set.

Let $P_0 = \text{Bern}(p)$, $P_1 = \text{Bern}(p + \beta)$, with $p = \alpha_{\min}$. For any test φ , the Bretagnolle–Huber form of Le Cam’s inequality gives

$$P_0^{\otimes m}(\varphi = 1) + P_1^{\otimes m}(\varphi = 0) \geq \frac{1}{2} \exp(-m \text{KL}(P_0 \| P_1)).$$

If both type-I and type-II errors are at most δ , the left-hand side is at most 2δ , hence

$$m \text{KL}(P_0 \| P_1) \geq \log \frac{1}{4\delta}.$$

A standard local Bernoulli KL bound gives, for $0 < \beta \leq \frac{1}{2} \min\{p, 1 - p\}$,

$$\text{KL}(\text{Bern}(p) \| \text{Bern}(p + \beta)) \leq \frac{2\beta^2}{p(1 - p)}.$$

Combining the two displays gives

$$m \geq \frac{p(1-p)}{2\beta^2} \log \frac{1}{4\delta}.$$

It remains to relate $p(1-p)$ to $\alpha(1-\alpha)$. Under the proposition's assumption $\beta \leq \frac{1}{2} \min\{p, 1-p\}$, we have $\alpha = p + \beta \leq 3p/2$ and $1 - \alpha = 1 - p - \beta \geq (1-p)/2$; together with $\alpha \geq p$ and $1 - \alpha \leq 1 - p$, this gives $\alpha(1-\alpha) \in [p(1-p)/2, (3/2)p(1-p)]$. Hence $p(1-p)$ and $\alpha(1-\alpha)$ differ by at most a factor of three, and substituting $m = \lfloor nq \rfloor$ yields (2) after adjusting the universal constant c . \square

B.5 Theorem 3 (distribution-dependent partition lower bound)

For the population lower bound, condition on the cell G_g and observe that on each cell the partition router plays a_g^* , the cell-optimal action, so its conditional loss is $\mathbb{E}[\ell(x, a_g^*) \mid x \in G_g]$. Averaging over cells,

$$\Delta_{\text{partition}}(\mathcal{G}) = \sum_g p_g (\mathbb{E}[\ell(x, a^*) \mid x \in G_g] - \mathbb{E}[\ell(x, a_g^*) \mid x \in G_g]) = \sum_g p_g \gamma_g.$$

Each summand is non-negative because a_g^* minimizes conditional loss on G_g , so $\Delta_{\text{partition}}(\mathcal{G}) \geq \max_g p_g \gamma_g$, which is (3).

For the sample-complexity statement, condition on the partition and let $M_g \sim \text{Binom}(n_{\text{tr}}, p_g)$ be the realized training-fold count on cell G_g , with $n_{\text{tr}} = (\kappa - 1)n/\kappa$ and mean $\bar{m}_g = n_{\text{tr}} p_g$. Because Bernstein's bound is convex in $1/m_g$, substituting \bar{m}_g directly is not rigorous; we first lower-bound M_g by a multiplicative Chernoff inequality, $\mathbb{P}(M_g \geq \bar{m}_g/2) \geq 1 - \exp(-\bar{m}_g/8)$, then condition on this event with $\delta/2$ budget. On it, Bernstein's inequality applied to each action's empirical mean on cell G_g with variance at most σ^2 and range at most L_{\max} gives

$$\mathbb{P}(|\widehat{L}_g(a) - L_g(a)| \geq t) \leq 2 \exp\left(-\frac{(\bar{m}_g/2) t^2}{2\sigma^2 + (2/3)L_{\max} t}\right).$$

Union-bounding over the $|\mathcal{A}|$ actions with the remaining $\delta/2$ budget, the empirical argmin's Bernstein deviation is at most $\gamma_g/2$ on every action whenever $\bar{m}_g \geq (16\sigma^2 + (8/3)L_{\max}\gamma_g) \log(4|\mathcal{A}|/\delta)/\gamma_g^2$, in which case $\widehat{L}_g(\widehat{a}_g^*) \leq \widehat{L}_g(a_g^*) \leq L_g(a_g^*) + \gamma_g/2$ and therefore $L_g(\widehat{a}_g^*) \leq L_g(a_g^*) + \gamma_g = L_g(a^*)$, so the empirical Π_1 estimator's cell loss is no worse than the global baseline on cell G_g . Substituting $\bar{m}_g = (\kappa - 1)np_g/\kappa$ and rearranging gives the stated bound. Strictly, the requirement is $\bar{m}_g \geq \max\{8 \log(2/\delta), (16\sigma^2 + (8/3)L_{\max}\gamma_g) \log(4|\mathcal{A}|/\delta)/\gamma_g^2\}$, where the first term is the Chernoff floor on cell occupancy and the second the Bernstein concentration term, matching the explicit max in the theorem statement; the Bernstein term dominates whenever γ_g is bounded away from L_{\max} . \square

B.6 Theorem 4 (held-out selection bound)

Let $M = |\mathcal{M}|$ be the number of candidate classes. For each class $m \in \mathcal{M}$, the inner κ -fold CV estimate $\widehat{R}_{\text{CV}}(m)$ is the average of held-out-fold empirical risks, with each held-out fold containing $n_{\text{in}} = n_{\text{out}}/\kappa$ samples and loss bounded in $[0, L_{\max}]$. Treating the fold-trained estimator as fixed conditional on its training split, Hoeffding's inequality gives the displayed deviation rate for each held-out fold; averaging over folds preserves the same order. Thus, for the inner-CV estimand $\bar{R}_\kappa(m)$,

$$\mathbb{P}(|\widehat{R}_{\text{CV}}(m) - \bar{R}_\kappa(m)| > t) \leq 2 \exp\left(-\frac{2 n_{\text{in}} t^2}{L_{\max}^2}\right),$$

where $\bar{R}_\kappa(m) := \mathbb{E}_{S'}[R(\widehat{\pi}_m(S'))]$ is the expected risk of the estimator trained on a single inner-training fold of size $n_{\text{out}}(\kappa - 1)/\kappa$. A union bound over the M candidate classes gives

$$\mathbb{P}\left(\max_m |\widehat{R}_{\text{CV}}(m) - \bar{R}_\kappa(m)| > t\right) \leq 2M \exp\left(-\frac{2 n_{\text{in}} t^2}{L_{\max}^2}\right).$$

Define the threshold $t^* := L_{\max} \sqrt{\log(2M)/(2n_{\text{in}})}$, at which the right-hand side of the union bound equals 1. On the event that all class deviations are at most some t , the selection $\widehat{m} = \arg \min_m \widehat{R}_{\text{CV}}(m)$ satisfies

$$\bar{R}_\kappa(\widehat{m}) \leq \widehat{R}_{\text{CV}}(\widehat{m}) + t \leq \widehat{R}_{\text{CV}}(m^*) + t \leq \bar{R}_\kappa(m^*) + 2t$$

for any competitor class m^* . Taking expectations through tail integration $\mathbb{E}[Z_+] = \int_0^\infty \mathbb{P}(Z > x) dx$ applied to $Z = \bar{R}_\kappa(\hat{m}) - \min_m \bar{R}_\kappa(m)$: the integrand is at most 1 for $t \leq t^*$ (contributing $2t^*$ after the factor-of-2 chaining above) and at most $2M \exp(-2n_{\text{in}}t^2/L_{\text{max}}^2)$ for $t > t^*$ (a Gaussian tail bounded by $L_{\text{max}}/(2\sqrt{2n_{\text{in}} \log(2M)}) \leq t^*$ for $M \geq 2$). Both contributions are at most $2t^*$, giving

$$\begin{aligned} \mathbb{E}[\bar{R}_\kappa(\hat{m})] &\leq \min_{m \in \mathcal{M}} \bar{R}_\kappa(m) + 4t^* = \min_{m \in \mathcal{M}} \bar{R}_\kappa(m) + 2\sqrt{2} L_{\text{max}} \sqrt{\frac{\log(2|\mathcal{M}|)}{n_{\text{in}}}} \\ &\leq \min_{m \in \mathcal{M}} \bar{R}_\kappa(m) + 4L_{\text{max}} \sqrt{\frac{\log(2|\mathcal{M}|)}{n_{\text{in}}}}. \end{aligned}$$

If refitting a selected class from inner-training size to the full outer-training size changes its expected risk by at most $\varepsilon_{\text{stab}}(n_{\text{out}}, \kappa)$, and the same holds for the best competitor class, the refit bound follows by adding $2\varepsilon_{\text{stab}}(n_{\text{out}}, \kappa)$. \square

C Setup and implementation

This appendix details the implementation. Section C.1 specifies the per-benchmark feature blocks; Section C.2 the loss matrix and the diagnostic constants L_r, L_w, L_a ; Section C.3 the controller family pool and the cost-sensitive L2D adaptations; Section C.4 the strict nested-CV protocol and the retrieve-action prompting.

C.1 Feature block specification

For HallusionBench and A-OKVQA the controller consumes a fixed scalar feature block of 41 dims (HallusionBench) or 39 dims (A-OKVQA), built entirely from the upstream Qwen2.5-VL prediction-time outputs (per-action margins, agreements, sampled-completion statistics, modality-bypass probes, and self-verification probes); the InternVL2.5-8B judge is used *only* to populate the semantic-risk channel of the loss matrix (Appendix C.2) and never enters the feature block. FOLIO uses a 12-dimensional simplified block constructed from the same Qwen2.5-VL outputs in text-only mode (described at the end of this subsection). SMS-Spam uses a 12-dimensional TF-IDF-based block (Appendix D.1). The TextVQA-OCR add-on uses a separate non-OCR feature block (exposed to Π_0, Π_1, Π_2 ; OCR-derived features go only to Π_3): three scalars (direct-confidence, question length in tokens, number of image classes) plus one-hot indicators (the first question token, the first 12 question tokens, tokens matching a small fixed text-key vocabulary, and the first 8 image-class names), assembled via a sparse DictVectorizer so the realized width is vocabulary-dependent. The Π_3 prior block additionally exposes OCR-derived signals (OCR confidence/margin, prediction length and digit/year flags, question/prediction overlap, training-frequency log) under the deterministic OCR-confidence gate. The hallucination/VQA block is organized into six groups, each of which expands to multiple scalars:

1. *Per-action confidence and margin* (7 dims). For each of the three non-abstain actions (direct, retrieve, defer): the greedy softmax margin and the mean per-token log-probability of the generated answer. Additionally, a context-aware margin for the retrieval action. These features capture first-order output-distribution signals for every candidate action.
2. *Cross-action agreement* (3 dims). Pairwise token-level agreement between the answers produced by direct, retrieve, and defer (agree_dr, agree_de, agree_re; the suffix letters are implementation identifiers and predate this paper’s terminology).
3. *Question metadata* (2 dims). Question length in words and cosine similarity between question and context embeddings.
4. *Semantic similarity and benchmark categories* (8 dims on HallusionBench, 10 on A-OKVQA). Pairwise cosine similarities among the sentence embeddings of the three action-specific answers and between each answer and the question (6 pairs), plus benchmark-specific categorical one-hot indicators (HallusionBench: 2 dims, VD/VB category; A-OKVQA: 4 dims, question-type).
5. *Stochastic-sampling uncertainty* (8 dims, from $K=10$ sampled completions). Self-consistency count ratio (max-answer frequency divided by K), sample disagreement, Shannon semantic entropy over parsed distinct answers, predictive entropy from the first-token softmax, and means

and standard deviations of the per-sample softmax margin and sequence log-probability across the K draws.

6. *Verification and modality-bypass probes* (13 dims on HallusionBench, 9 on A-OKVQA). Five scalars from a modality-bypass (image-blanked) probe applied to the vision benchmarks: a binary disagreement flag, softmax margin, sequence log-probability, $P(\text{yes}) - P(\text{no})$, and top-1 token probability. Plus four scalars from a 3B self-verification re-ask ($P(\text{yes})$, $P(\text{no})$, their difference, and a binary text-contains-yes flag); on HallusionBench this is repeated under the 7B re-asker, contributing four further scalars ($P(\text{yes})$, $P(\text{no})$, their difference, and the binary text-contains-yes flag).

All features are computed once per sample on the upstream pipeline and represented as a dense matrix paired with the loss matrix. Features are standardized per outer-training fold via `sklearn.preprocessing.StandardScaler`, and all AUCs reported in Table 2 are computed with `sklearn.metrics.roc_auc_score` on the concatenation of outer-test folds so that the reported α_{emp} reflects the same data budget the controllers see.

The FOLIO 12-d block is built from groups 1–2 above (no $K=10$ stochastic, no blind-probe, no self-verification, no InternVL features, no question metadata) plus two predicted-label indicators (`pred_true`, `pred_uncertain`): per-action confidence margin and sequence log-prob (6 dims), three pairwise agreements (3 dims), the recover-context margin (1 dim), and the two indicator features (2 dims). This deliberately constrained block is part of the variance-bounded regime instantiation: Theorem 2’s threshold $n_{\text{min}} \propto \alpha(1-\alpha)/\beta^2$ depends on the AUC the feature block can extract, so a thinner block at small n instantiates the Cor 1 (ii) sub-case where Π_2 ’s sign is uncertified.

C.2 Loss matrix construction

Loss components and per-benchmark labeling. The per-sample loss $\ell(x_i, a)$ is constructed from three operational quantities. Correctness $c(x_i, a) \in \{0, 1\}$ is evaluated against the benchmark gold label. Operational cost $k(x_i, a)$ is measured in action-cost units (1.0 for direct, 2.0 for retrieve, 2.3 for defer, 0.0 for abstain). Semantic risk $h(x_i, a) \in \{0, 0.5, 1\}$ is a per-action grounded-support label: $h=0$ (grounded), 0.5 (unverifiable), 1.0 (contradicted), with $h=0$ for a_{abstain} by construction. Labeling is benchmark-specific and run offline. *HallusionBench* and *A-OKVQA*: each (sample, action) candidate answer’s most specific visual proposition is extracted and classified against image evidence by an InternVL2.5-8B judge as grounded / unverifiable / contradicted. *FOLIO* uses a rule-based proxy ($h=0.5$ if the action’s answer disagrees with the gold label, $h=0$ if it agrees), keeping the loss matrix simple while still exposing wrong answers to a calibrated penalty; using a learned NLI judge here would conflate the controller’s behaviour with the judge’s quality on logical inference. *SMS-Spam* uses canonical-cost weighting without a separate judge (Appendix D.1).

Headline formula and weight robustness. The headline core loss is

$$\ell(x_i, a) = 1.0 \cdot (1 - c(x_i, a)) + 1.0 \cdot h(x_i, a) + 0.05 \cdot k(x_i, a),$$

which is the exact formula used for the four core benchmarks throughout this paper. Abstention therefore has loss 1.0, because it is treated as an always-incorrect zero-risk zero-cost action. Since this weight vector is a cost-sensitive operating point, Table 7 reruns the deployable $\Pi_0/\Pi_1/\Pi_2$ pool under local one-factor perturbations of these weights: $w_c \in \{0.75, 1.0, 1.25\}$, $w_h \in \{0.75, 1.0, 1.25\}$, and $w_k \in \{0.025, 0.05, 0.10\}$, varying one coordinate at a time around (1, 1, 0.05). The TextVQA-OCR add-on instead uses answer loss 1–soft-VQA accuracy because the experiment isolates OCR copying rather than semantic-risk/cost tradeoffs.

Diagnostic constants and numerical examples. The quantities $L_r := \mathbb{E}[\ell(x, a_{\text{direct}}) \mid c_{\text{direct}}=1]$, $L_w := \mathbb{E}[\ell(x, a_{\text{direct}}) \mid c_{\text{direct}}=0]$, and $L_a := \mathbb{E}[\ell(x, a_{\text{abstain}})]$ are computed as simple sample means over the respective subsets of the full core benchmark for the Π_2 viability diagnostic; they are global (not fold-specific) constants for each benchmark, so $\alpha_{\text{min}} = (L_a - L_r)/(L_w - L_r)$ is a single number per benchmark that does not depend on the CV fold. For scale, the `always_direct` losses decompose under this formula as HallusionBench $1.0848 = (1 - 0.6685) + 0.7033 + 0.0500$, A-OKVQA $0.4138 = (1 - 0.8306) + 0.1944 + 0.0500$, and FOLIO $0.7520 = (1 - 0.5320) + 0.2340 + 0.0500$. Correctness c is gold-evaluated and therefore identical across judge choices; on HallusionBench and A-OKVQA the per-action risk h values entering Table 1 come from the

InternVL2.5-8B judge from a different VLM family than the upstream Qwen2.5-VL policies, so the judge does not score outputs from its own family. On HallusionBench the population-mean per-action losses are (1.085, 1.136, 1.104, 1.000) for (direct, retrieve, defer, abstain), so abstain becomes the best fixed action by a wide margin and the `fair_fixed_train` CV variant reliably recovers it; on A-OKVQA and FOLIO direct remains the best fixed action on outer-test. Table 1’s Π_0 column reports the strict-CV-selected variant on each benchmark.

C.3 Family pool and baseline implementations

Our family pool is evaluated through a `uniform fit(X, L, C)/predict(X)` interface in the strict nested CV pipeline. Π_0 holds `always_direct` and a fair-fixed CV variant. Π_1 (KMeans) uses KMeans routers with $K \in \{4, 5, 6, 8\}$ on the standardized feature block, with per-cell action assigned by conditional loss argmin on outer-train and a global-best fallback for cells with fewer than three training samples. An alternative Π_1 (CART) realization uses `DecisionTreeClassifier` with `max_depth` $\in \{3, 4\}$ and `min_samples_leaf` = 5, fit on per-sample loss-argmin labels with the same per-leaf override and small-cell fallback (Table 6). Π_2 uses `HistGradientBoostingClassifier` (`max_depth` $\in \{3, 4\}$) and a calibrated logistic plug-in ($C=0.3$, referred to as `Selective-C=0.3` elsewhere in this paper), with each family predicting a four-action argmin from the feature block.

We additionally evaluate two cost-sensitive adaptations of canonical learning-to-defer baselines through the same interface. The Mozannar–Sontag adaptation [Mozannar and Sontag, 2020] is a row-replicated multinomial logistic regression: each training row x_i is replicated $|\mathcal{A}| = 4$ times with the action index as the label and a sample weight $w_{i,a} = L_{\max,i} - L[i, a]$ encoding the cost margin, with L_2 regularization $C \in \{0.3, 1.0\}$; at test time we predict the softmax argmax. The Narasimhan adaptation [Narasimhan et al., 2022] is a post-hoc plug-in: one `HistGradientBoostingRegressor` per action (`max_iter` = 200, `max_depth` $\in \{3, 4\}$, `learning_rate` = 0.05) is trained on the per-action loss column, and the test policy is $\pi(x) = \arg \min_a \widehat{L}_a(x)$. Both are loss-matrix-compatible cost-sensitive instantiations rather than reproductions of the original human-deferral objectives; their detailed strict-CV results are in Appendix F.1.

C.4 Evaluation protocol and reproducibility

Strict nested CV. All headline tables use strict nested 5-fold-by-5-seed cross-validation with family selection on outer-train only, followed by a refit of the selected family on outer-train only and a single evaluation on outer-test. Non-strict variants that refit on outer-train-plus-outer-test are excluded from the canonical results: in pre-paper diagnostic runs on HallusionBench’s best Π_2 family the non-strict refit produced losses inflated by ~ 0.1 relative to the strict variant, the textbook overfit signature of refitting on the evaluation fold. Families, hyperparameter grids, and seeds are fixed; the strict outer CV is deterministic given the fixed seeds and pre-computed loss matrix.

Retrieve action. The a_{retrieve} action on HallusionBench, A-OKVQA, and FOLIO is generated by the same upstream model (Qwen2.5-VL-3B-Instruct) under a grounded-context prompting pass: a single forward call instructs the model first to enumerate scene context literally (objects, attributes, relations on visual benchmarks; key facts and entities on FOLIO) and then to commit to the question’s answer conditional on that enumeration, with the final commitment extracted by deterministic regex from the response. There is no external retrieval corpus; the “retrieved” context is the model’s own free-form description, so a_{retrieve} costs one extra forward pass over a_{direct} but draws on no information unavailable to the upstream model.

Hardware. All experiments run on AMD EPYC 7543 CPU cores and a single NVIDIA A100 GPU.

D Per-benchmark details

Each subsection below applies Corollary 1 to one core benchmark, starting with the predicted regime and then giving empirical detail beyond the main text.

D.1 SMS-Spam: residual-bounded witness for Theorem 1

The SMS-Spam Collection [Almeida et al., 2011] is a 5,574-message English binary classification corpus (ham vs. spam). We use a deterministic 80/20 split ($n_{\text{train}}=4460$, $n_{\text{test}}=1114$; seed-0 NumPy permutation) and CPU-only TF-IDF features. The three deployable actions are: *direct* = TF-IDF (1,2)-gram (max_features 50,000, min_df 2) + calibrated LinearSVC ($C=1.0$, 3-fold sigmoid calibration), 0.9910 test accuracy; *retrieve* = TF-IDF (1,1)-gram (max_features 20,000, min_df 2) + KNN ($k=10$, cosine), 0.9811; *defer* = same TF-IDF (1,1)-gram + logistic regression ($C=1.0$), 0.9758. The 12-d scalar feature block is per-action top-1 minus top-2 probability, per-action top-1 log-probability, three pairwise prediction agreements, and 3 TruncatedSVD components fit on the SMS training split’s (1,2)-gram TF-IDF matrix and applied to the held-out split. Loss uses canonical core weights (1, 1, 0.05) and the same {1.0, 2.0, 2.3, 0.0} action-cost vector as the other core benchmarks; abstain has zero operational cost k and (per the convention in Section 2.1) loss 1.0 under the canonical correctness weight.

This configuration deliberately instantiates the residual-bounded regime: the bigram + calibrated SVC direct is task-specialized, while the unigram logistic-regression defer is generic and not stronger on this task. We measure the four diagnostics from Section 2.2 and Theorem 1: $\mathbb{P}(R)=0.009$, oracle Π_2 gain =0.003, oracle Π_1 partition gain =0.000 (over a post-hoc $K \in \{2, 3, 4, 5, 6, 8\}$ KMeans sweep on an SVD-8 diagnostic embedding), and the local tail-margin condition of Lemma 1 fails: $\mathbb{P}(R) = 0.009$ caps the bottom- q precision by $\mu_w(q) \leq \mathbb{P}(R)/q \leq 0.03$ for $q \geq 0.3$, below $\alpha_{\text{min}} = 0.95$ (abstain fallback) and $\alpha_{\text{min}} = 0.089$ (defer fallback), so no rejector improves on a_{direct} asymptotically. We record this as $\beta \leq 0$ in Table 2 under the AUC scalar-proxy convention. All four are below the residual-bounded thresholds (< 0.02 , < 0.005 , < 0.005). Theorem 3 sharpens the Π_1 diagnostic: $\max_g p_g \gamma_g = 0$ means every cluster’s cell-best action coincides with the global-best a_{direct} , so $\pi_1^* \in \Pi_0$ at the population level. Under strict nested 5-fold-by-5-seed CV, every Π_1 family (KMeans- $K \in \{4, 5, 6, 8\}$) collapses to direct ($\Delta = +0.0000$), the best Π_2 family is SelectiveCalibrated_C0.3 at 0.0591 ± 0.0000 ($\Delta = +0.0002$), and the two HGBC families lose by $\Delta \in \{+0.0007, +0.0011\}$ to the fixed action—the predicted ordering $\Pi_0 \leq \Pi_1 \leq \Pi_2$ up to multi-seed noise.

A simple structural lower bound on $\mathbb{P}(R)$ explains why this regime is rare under standard deferral setups. If defer’s accuracy exceeds direct’s by $\delta > 0$, then $\mathbb{P}(R) \geq \delta$ (the direct-wrong/defer-correct samples already form a δ -fraction). Under the canonical defer cost premium $0.05(c_{\text{defer}} - c_{\text{direct}}) = 0.065$, residual loss is bounded only when δ is comparable to or below this premium. The other three core benchmarks all have substantial residual mass: HallusionBench (defer-direct accuracy gap $\delta=0.037$) and A-OKVQA ($\delta=0.034$) violate the structural lower bound by defer’s accuracy advantage; FOLIO ($\delta = -0.015$, defer slightly weaker) instead has $\mathbb{P}(R)=0.175$ driven by partition-level abstain dominance on its Uncertain subgroup. All three sit outside Theorem 1’s scope; SMS-Spam, with a generic and weaker fallback that produces neither a defer-side accuracy advantage nor a partition-level abstain region, satisfies it. The witness is therefore not a property of the corpus alone but of the cost-tiered configuration in which the fallback is non-specialized—which is the deployment regime Theorem 1 is meant to characterize.

D.2 HallusionBench: instance-level wins on the high-signal Bernstein-viable regime

Under the InternVL2.5-8B judge, HallusionBench at the full $n=920$ corpus is comfortably above the Bernstein threshold ($n_{\text{min}}^{\text{Bern}}=23$, with $n\beta^2=202$; Theorem 2); both Π_1 (best KMeans- $K=8$, 0.091 loss reduction) and Π_2 (best HGBC-md3, 0.103 loss reduction) beat the fixed action, with Π_2 edging Π_1 by ≈ 3 seed-sd of Π_2 . The deployable winner is therefore Π_2 ; Π_1 remains a useful lower-complexity diagnostic for Theorem 3. Figure 4 reports the partition anatomy at the simplest router ($K=4$, seed 42): InternVL2.5-8B’s stricter judging of direct-wrong samples makes a_{abstain} the global best fixed action under the canonical loss matrix (mean direct loss 1.085 vs. abstain’s 1.000), so by the definition $\gamma_g = \mathbb{E}[\ell(x, a^*) - \ell(x, a_g^*) \mid x \in G_g]$ a cluster contributes positively only when its cell-best action differs from $a^*=a_{\text{abstain}}$. One cluster carries essentially all the partition gain at $K=4$: cluster 0 ($p_0=0.274$) prefers a_{direct} with $\gamma_0=0.170$, contributing $p_0\gamma_0=0.047$; the remaining three clusters all prefer a_{abstain} and contribute zero, so $\max_g p_g \gamma_g = \sum_g p_g \gamma_g = 0.047$. The strict-CV empirical KM- $K=4$ loss reduction is 0.048 ± 0.005 relative to the fair_fixed_train baseline of 1.000, within sampling noise of $\sum_g p_g \gamma_g$: Theorem 3’s lower bound is empirically tight at $K=4$. The instance-level recoverable margin (HGBC-md3 at 0.103) exceeds this partition ceiling, so Π_2

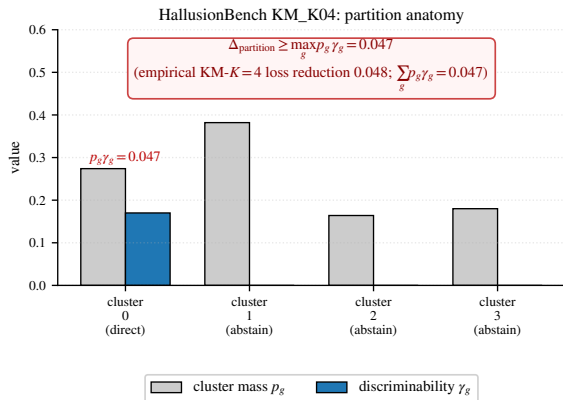


Figure 4: Cluster anatomy of HallusionBench KM- $K=4$, seed 42, witnessing Theorem 3. Under the canonical loss matrix the global best fixed action is abstain; only cluster 0 ($p_0=0.274$) carries positive discriminability by preferring direct ($\gamma_0=0.170$), contributing $p_0\gamma_0=0.047$. The empirical strict-CV KMeans- $K=4$ loss reduction is 0.048, within sampling noise of $\sum_g p_g\gamma_g=0.047$; the bound is empirically tight at $K=4$ on HallusionBench.

wins on HallusionBench by Corollary 1 item (iii)’s ceiling comparison, with the partition diagnostic confirming that Π_1 ’s gain is concentrated in a single direct-preferring subgroup rather than diffused across the partition.

D.3 A-OKVQA: deployable Π_2 winner with Π_1 boundary

A-OKVQA at full $n=1145$ is the deployable Π_2 winner (Table 1, Selective $C=0.3$ at -0.033 versus best Π_1 KMeans- $K=4$ at -0.024), but with the high-signal Π_1/Π_2 auto-pick boundary characteristic of Corollary 1 item (iii) when the two ceilings are commensurate: $C_{\Pi_2} = q^*\beta(L_w - L_r) \approx 0.094$ vs. $C_{\Pi_1} = \max_K \sum_g p_g\gamma_g \approx 0.039$ predicts Π_2 , but the recovered empirical margins are within one seed-sd of each other and inner-CV splits $\Pi_1:\Pi_2$ as 10:15 over 25 outer-folds (Appendix F.3). To complement this deployable result, Appendix D.4 reports a gold-rationale oracle that uses an answer-derived channel and is therefore not deployable; it pins down the Π_3 -style ceiling that an external prior could in principle reach.

D.4 A-OKVQA: gold-rationale Π_3 oracle (non-deployable)

A-OKVQA contains three human-written rationales per sample, outside the v10 scalar block. Because these rationales were collected after the answers and ask workers to explain why the correct answer is correct [Schwenk et al., 2022], they are answer-derived and not deployable side information. We treat the following as a gold-rationale *oracle experiment*: it measures the upper-bound value of an answer-derived explanatory channel, not a deployable Π_3 result.

We define a parameter-free binary gate $\rho(x)$ that fires when any content word of the model’s direct answer appears in any rationale of x . On A-OKVQA ρ fires on 806/1145=70.4% of samples with empirical direct-correct rate 94.4% inside the fired set (vs. base rate 83.1%); on the remaining 29.6% the rate collapses to 56.0%, giving AUC 0.784. The Π_3 -style family plays a_{direct} when $\rho=1$ and uses a KMeans- $K=4$ fallback on the non-fire subset, with no tunable hyperparameters.

Under strict 5-fold-by-5-seed CV the oracle reaches 0.3554 ± 0.0019 , beating the best scalar Π_1 at 0.3902 ± 0.0085 by -0.0348 and the best scalar Π_2 at 0.3805 ± 0.0032 by -0.0251 , gaps of about 4 and 7 seed-sd units, respectively. The result is numerically consistent with the region where Π_3 wins in Appendix E.3; the gate’s AUC matches the high-prior-signal region. However, the channel itself is answer-derived, so the experiment serves as motivation for label-free Π_3 channels (OCR, retrieval, knowledge bases) rather than a deployable A-OKVQA Π_3 result.

A-OKVQA ($n=1145$), best Π_2 per block	loss	std	Δ vs Π_3
<i>Canonical v10 scalar block (39-d), no rationale access</i>			
Π_0 : always_direct	0.4138	0.0000	+0.0584
Π_1 : KMeans- $K=4$	0.3902	0.0085	+0.0348 (4.0 seed-sd)
Π_2 : SelectiveCalibrated $C=0.3$	0.3805	0.0032	+0.0251 (6.8 seed-sd)
<i>Π_2 given progressively richer rationale representations</i>			
Π_2 HGBC-md3 + exact-match (40-d)	0.3749	0.0052	+0.0195 (3.5 seed-sd)
Π_2 HGBC-md3 + text-overlap stats (45-d)	0.3737	0.0045	+0.0183 (3.7 seed-sd)
Π_2 HGBC-md3 + TF-IDF top-200 (239-d)	0.3847	0.0043	+0.0293 (6.2 seed-sd)
<i>Π_3-style gold-rationale oracle (not a deployable feature)</i>			
Π_3 oracle: rationale gate + KM- $K=4$ fallback	0.3554	0.0019	0 (oracle)

Table 4: Gold-rationale oracle decomposition on A-OKVQA (5-seed strict CV). **Top:** scalar-only deployable families. **Middle:** Π_2 HGBC given three progressively richer learned representations of the rationale channel. **Bottom:** the deterministic gold-rationale gate plus KMeans fallback. None of the three augmented Π_2 variants closes the gap to the oracle gate (3.5–6.2 seed-sd above), and each row reports the lowest-mean Π_2 family within its block.

D.5 FOLIO: variance-bounded witness for Corollary 1 (ii)

FOLIO [Han et al., 2024] is a 203-sample first-order-logic NLI benchmark in which each example consists of 1–7 premises and a conclusion, with a 3-way label (True / False / Uncertain) at $\approx 35:30:34\%$. We use the official validation split in full ($n=203$) and the same Qwen2.5-VL-3B-Instruct ($a_{\text{direct}}, a_{\text{retrieve}}$) and Qwen2.5-VL-7B-Instruct (a_{defer}) backbones in text-only mode, with rule-based per-action risk ($h=0.5$ if action’s answer is wrong, $h=0$ otherwise). The 12-d feature block is per-action confidence margin, sequence log-prob, recover-context margin, three pairwise agreements, and two indicator features for the model’s predicted-label class.

The full- n quantities are $\alpha_{\text{emp}}=0.687$, $\alpha_{\text{min}}=0.633$, so $\beta \approx 0.0528$ (displayed as 0.053 to three decimals throughout) and $n_{\text{min}}^{\text{Bern}}=1898$ from the leading-order formula at the unrounded β . FOLIO is therefore $\approx 9.4\times$ below the Bernstein threshold: Theorem 2 does *not* certify the sign of the empirical Π_2 loss difference, and Corollary 1 item (ii) predicts that whenever $\max_g p_g \gamma_g > 0$ a partition router strictly improves on Π_0 while Π_2 may have wrong sign. Both predictions hold empirically: the deployable Π_1 winner KMeans- $K=6$ reaches 0.7195 ± 0.007 versus Π_0 ’s 0.7520 (a 0.0325 reduction, 4.5 seed-sd of Π_1); the deployable Π_2 winner Selective- $C=0.3$ reaches 0.7546 ± 0.009 , +0.0027 worse than Π_0 , exactly the uncertified-sign behaviour Corollary 1 (ii) predicts when $n \ll n_{\text{min}}^{\text{Bern}}$.

The partition’s anatomy is unbalanced and concentrated. The KMeans clustering recovers eight clusters at $K=8$; only three carry positive discriminability (the three clusters whose cell-best action is not the global best fixed action), with $p_g \gamma_g$ contributions 0.006, 0.012, 0.047 summing to $\sum_g p_g \gamma_g = 0.065$. The empirical KM- $K=6$ loss reduction 0.0325 is below this oracle ceiling because (i) strict-CV refits KMeans on each outer-train fold of size ~ 162 , smaller than the full-pool seed-42 partition, and (ii) the ceiling assumes oracle cell-best actions whereas the empirical estimator must learn them. Π_2 ’s wrong-sign behaviour is structurally driven: with $\beta=0.053$ the canonical Π_2 asymptotic ceiling is only $q^* \beta (L_w - L_r) \approx 0.024$, which by Theorem 2 requires $n \geq 1898$ to be reliably recovered; at $n=203$ the variance overhead exceeds the ceiling. Theorem-driven prediction (Π_1 winner; Π_2 uncertified) and empirical realization match without further tuning.

E Controlled synthetic validation

We complement the per-benchmark results with three controlled synthetics that hold all but one structural variable fixed and sweep only the relevant diagnostic: Section E.1 sweeps n across the Bernstein viability threshold of Theorem 2; Section E.2 varies instance-level signal at fixed partition gap to test the Π_1/Π_2 phase transition (Cor 1 (iii)); Section E.3 varies an external prior channel’s informativeness to characterize when Π_3 wins.

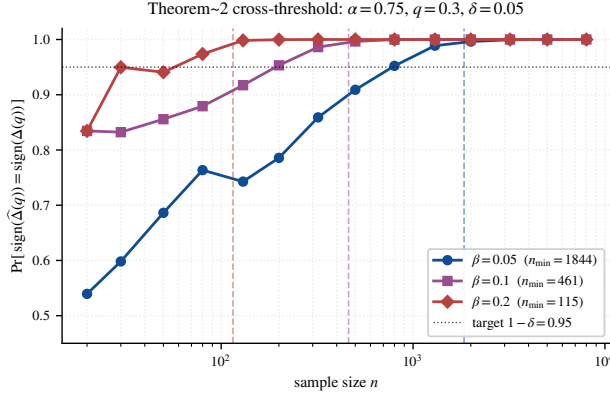


Figure 5: Bottom- q precision-estimator cross-threshold. At each β , the empirical sign-correctness rate (over 4000 replications per cell) reaches the target $1 - \delta = 0.95$ (dotted black) at sample sizes consistent with, and somewhat below, the predicted threshold $n_{\min}(\beta)$ (dashed vertical lines). The empirical curves are consistent with the order-tight β^{-2} scaling guaranteed by Proposition 1 but show the constant slack typical of Bernstein-style sufficient conditions; the synthetic does not run the full Π_2 /CV pipeline and so does not directly verify constant-tightness in deployed controllers. Above each n_{\min} the rate saturates at ≈ 1 ; below, it degrades smoothly as predicted by the variance-bounded sub-case of Corollary 1 (ii).

E.1 Bottom- q precision-estimator cross-threshold for Theorem 2

The four core benchmarks place a single point on each side of the Bernstein threshold (FOLIO below, HallusionBench/A-OKVQA above), but they cannot show how sign correctness behaves *as* n crosses n_{\min} . The synthetic in Section E.2 sweeps Π_1/Π_2 instead and stays above threshold throughout. We therefore include a dedicated cross-threshold experiment on the same bottom- q precision estimator that Theorem 2 analyses (not the full Π_2 /CV pipeline; see Appendix E.2 for that).

At fixed $(\alpha, q, \delta) = (0.75, 0.3, 0.05)$, we sweep $n \in \{20, 30, 50, 80, 130, 200, 320, 500, 800, 1300, 2000, 3200, 5000, 8000\}$ and $\beta \in \{0.05, 0.10, 0.20\}$ (so $n_{\min} \in \{1844, 461, 115\}$). For each (n, β) , we draw 4000 replications of the bottom- q precision estimator (each replication: $m = \lfloor nq \rfloor$ i.i.d. Bernoulli(α) draws under the local tail-margin convention) and record the empirical sign-correctness rate $\Pr[\text{sign}(\widehat{\Delta}(q)) = \text{sign}(\Delta(q))]$. Theorem 2 predicts this rate is at least $1 - \delta = 0.95$ once $n \geq n_{\min}(\beta)$.

Figure 5 shows the resulting rates. For each β , the empirical curve crosses the $1 - \delta$ target at a sample size at or somewhat below $n_{\min}(\beta)$, confirming the qualitative prediction (sign certified for $n \gtrsim n_{\min}$, uncertified below) and showing scaling consistent with order-tight β^{-2} separation. The displayed grid’s first empirical crossings sit at $n/n_{\min} \in [0.43, 0.69]$, the constant-factor gap typical between Bernstein-derived sufficient conditions and the actual finite-sample saturation point; Proposition 1 rules out improvement in the leading order, not in constants. FOLIO’s empirical wrong-sign Π_2 lands in the curve’s variance-bounded regime: its $n/n_{\min} = 203/1898 = 0.107$ ratio sits below all three empirical-saturation crossings, so the wrong-sign observation is robust to the constant slack of the Bernstein sufficient condition. The synthetic uses $\alpha = 0.75$ versus FOLIO’s $\alpha_{\text{emp}} = 0.687$, so the mapping is qualitative; HallusionBench at $n = 920$, $\beta = 0.469$ sits well past saturation.

E.2 Π_1/Π_2 phase transition for Corollary 1

The data-generating process has four latent clusters of mass $(0.35, 0.25, 0.20, 0.20)$ in \mathbb{R}^6 with a residual heterogeneity that gives Π_1 a fixed population partition gap of $\max_g p_g \gamma_g \approx 0.08$. A scalar knob $\text{bk} \in \{0, 0.5, 1.0, 1.6, 2.4, 3.5\}$ controls how much smooth continuous signal the features carry about c_{direct} : at $\text{bk} = 0$ the only information is cluster identity, and as bk grows a continuous feature is added that makes the discriminative signal increasingly extractable by a regularized LR classifier. We sweep $n \in \{150, 300, 600, 1200, 2400, 4800\}$ crossed with bk , run three seeds per cell with Π_1 realized as KMeans- $K=4$ and Π_2 realized as a regularized LR softmax (a deliberately compact

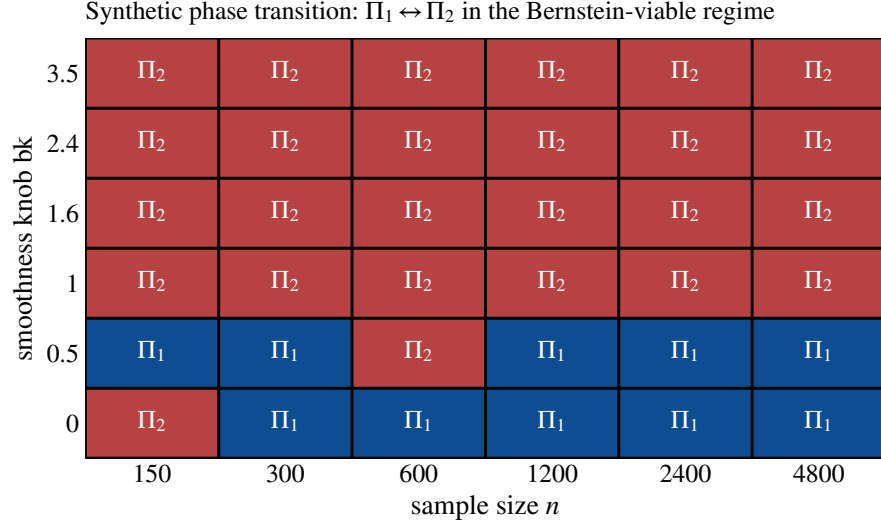


Figure 6: Controlled synthetic validation of Corollary 1 item (iii). Each tile is one (n, bk) cell colored by the empirical winner class (blue = Π_1 , red = Π_2). The partition gap is held fixed at $\max_g p_g \gamma_g \approx 0.08$; the smoothness knob bk on the y-axis is the only manipulated variable, and the resulting empirical margin β stays in $[0.37, 0.62]$ across all cells, well above the Bernstein viability threshold of Theorem 2, so this experiment is *not* a Theorem 2 validation. At low bk the only signal is cluster identity and Π_1 's direct per-cluster argmin beats Π_2 's regularized LR softmax; at higher bk the added smooth feature gives Π_2 enough instance-level margin to overtake the partition gap. The empirical winner boundary thus realizes the direct comparison between instance-level margin and partition gain that Corollary 1 item (iii) predicts.

subset of the main-paper Π_2 pool, isolating capacity-realization effects), and declare the winner class. Every cell in the sweep sits comfortably above the Bernstein viability threshold of Theorem 2 (since β stays in $[0.37, 0.62]$ throughout), so this experiment is *not* a Theorem 2 validation. It is a direct test of the population-versus-empirical clause in item (iii) of Corollary 1: when the asymptotic ceilings $C_{\Pi_2} > C_{\Pi_1}$ at every cell, does the empirical winner still track the comparison once a finite-capacity Π_2 family is plugged in? Figure 6 plots the resulting winner map.

The result is precisely the population-versus-empirical gap that the second clause of Corollary 1 (iii) anticipates. The asymptotic instance-level ceiling $C_{\Pi_2} = q^* \beta (L_w - L_r)$ exceeds the partition gap 0.08 at every cell since $\beta \in [0.37, 0.62]$ is large throughout, so the population-optimal clause of Cor 1 (iii) predicts Π_2 . The empirical winner does not always match: at $bk = 0$, when the only source of margin is discrete cluster identity, Π_1 beats Π_2 at every $n \geq 300$ because Π_1 's per-cluster argmin recovers the cell-best action sharply while the regularized LR family under-realizes the same discrete signal. As bk grows the LR family's recoverable margin rises (closer to its asymptotic ceiling), and once it overtakes the fixed partition gain the empirical winner flips to Π_2 and stays there: Π_1 wins 10/12 cells for $bk \in \{0, 0.5\}$ and Π_2 wins all 24/24 cells for $bk \geq 1$, with the two Π_2 wins at $(n=150, bk=0)$ and $(n=600, bk=0.5)$ within 0.003 of Π_1 (multi-seed noise). The synthetic therefore confirms that the empirical winner tracks the asymptotic-ceiling comparison only to the extent that the deployed Π_2 family realizes its ceiling; replacing the LR family with a higher-capacity Π_2 (HGBC), as in the main-paper pool, would shift the bk threshold but not the qualitative conclusion that ceiling comparison is mediated by family realization.

E.3 Π_3 orthogonal-channel sweep

Π_3 can strictly improve on lower classes only when a label-free external prior channel carries information about correctness beyond what the Π_2 feature block provides. To characterize this condition directly, we sweep the prior's informativeness in a controlled DGP.

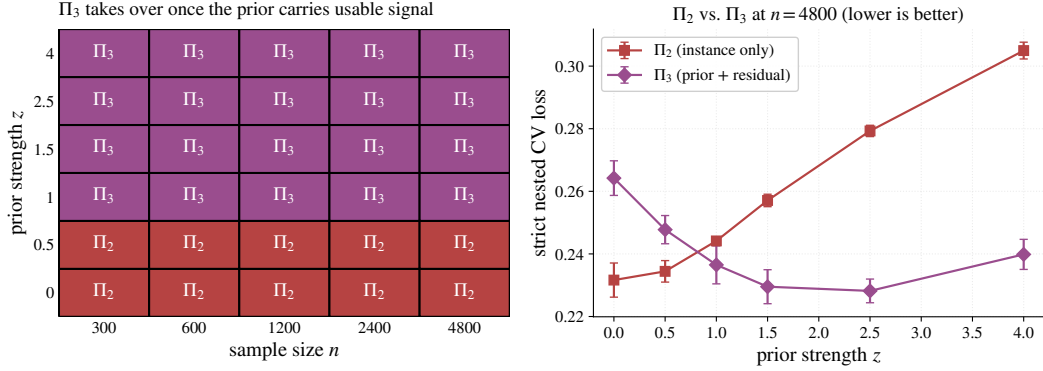


Figure 7: Controlled synthetic validation of Π_3 , with the partition signal weakened ($|\text{bump}| \leq 0.3$) and the Π_2 smooth-signal knob fixed at $\text{bk}=1.6$ so Π_2 sits comfortably in its high-signal regime. **Left:** empirical winner tile plot across (n, z) ; each cell is a strict nested 5-fold CV outcome colored by the winning class (red= Π_2 , purple= Π_3). At $z \in \{0, 0.5\}$ the prior is uncorrelated or only weakly correlated with correctness and Π_2 wins every cell (10/30); at $z \geq 1.0$ the prior carries enough signal about correctness that prior-gate decisions are more reliable than anything Π_2 can extract from X , and Π_3 wins every cell (20/30). **Right:** at $n=4800$, the Π_2 loss *grows* from 0.23 to 0.30 as z increases (the correctness logit becomes increasingly z -dominated and X correspondingly less informative), while the Π_3 loss falls from 0.26 at $z=0$ to the 0.23–0.24 band once $z \geq 1.0$. The separation between the two curves is the Π_3 gain.

Inputs are drawn from the same four-cluster Gaussian as in Appendix E.2, with the partition weakened ($\text{bump}=(+0.3, +0.3, +0.3, -0.3)$) and the Π_2 smooth-signal knob fixed at $\text{bk}=1.6$, so Π_2 sits comfortably in its high-signal regime. We add a hidden prior scalar $z \sim \mathcal{N}(0, 1)$ drawn independently of X , with correctness logit $\text{logit}(c_{\text{direct}}=1 \mid X, z) = \text{bk} s(X) + z_{\text{strength}} \cdot z + \text{bump}(g)$, where $s(X)$ is the unit-norm linear signal from Appendix E.2. The feature block exposed to Π_0, Π_1, Π_2 is X only; z is exposed exclusively to Π_3 . Because z is independent of X , no amount of Π_2 training on X can recover the information z carries about correctness, regardless of n .

Π_3 is implemented as the Definition 1 prior-gated controller with an explicit high-confidence gate: $\Pi_3(x, z) = a_{\text{direct}}$ if $z > \tau$, $\Pi_3(x, z) = a_{\text{defer}}$ if $z < -\tau$, and $\Pi_3(x, z) = r(x)$ otherwise, with $\tau=1.0$ so that the gate fires on the top/bottom $\approx 16\%$ of the prior and leaves the middle $\approx 68\%$ to the fallback. The asymmetric bump $= (+0.3, +0.3, +0.3, -0.3)$ keeps the partition discriminable so that the synthetic does not become trivially Π_3 -dominated by collapsing the Π_1 ceiling to zero. The fallback controller $r \in \Pi_2$ is a regularized multinomial logistic regression fit only on training samples with $|z_{\text{tr}}| \leq \tau$. We cross $n \in \{300, 600, 1200, 2400, 4800\}$ with $z_{\text{strength}} \in \{0, 0.5, 1.0, 1.5, 2.5, 4.0\}$, 3 seeds per cell, under the same strict 5-fold CV protocol.

The winner map (Figure 7 left) partitions the sweep into two regimes: when $z_{\text{strength}} \leq 0.5$ the prior is too weak to justify the gating cost and Π_2 wins uniformly in n ; when $z_{\text{strength}} \geq 1.0$ the prior is accurate enough that Π_3 's gated decisions dominate and Π_3 wins uniformly in n . The transition is crisp: there is no “ Π_3 wins at large n but not small n ” axis, because Π_3 's advantage comes from additional information rather than from more samples. The right panel anchors the mechanism on Π_3 : at $n=4800$, Π_3 's loss falls from 0.264 at $z_{\text{strength}}=0$ to the 0.23–0.24 band once $z_{\text{strength}} \geq 1.0$, showing that the gate becomes useful only after the prior carries enough signal; Π_2 's loss rises from 0.23 to 0.30 by construction of the DGP, since fixing $\text{bk}=1.6$ while raising z_{strength} makes X a relatively weaker driver of correctness, so the rising curve is a control rather than a finding. The displayed curves cross between $z_{\text{strength}} = 0.5$ and 1.0 (linear interpolation at $n=4800$ gives $z_{\text{strength}} \approx 0.82$), the operating point at which the prior carries enough signal that the certainty-on-the-tails gate outweighs the cost of routing the un-gated middle band to the fallback. The orthogonality $z \perp X$ is the cleanest possible setting for Π_3 and overstates the advantage available to a real channel that shares partial information with X ; the TextVQA-OCR experiment in Section 3 is the deployable partial-overlap test, and the A-OKVQA gold-rationale oracle in Appendix D.4 is numerically consistent but methodologically non-deployable because the channel is answer-derived.

Benchmark	Mozannar (best)	Narasimhan (best)	Best (ours)	Verdict
HallusionBench	0.9203 \pm 0.005	0.8990 \pm 0.007	0.8970 \pm 0.004 (Π_2)	Narasimhan ties HGBC (0.3 sd); Mozannar trails (3.6 sd)
A-OKVQA	0.3877 \pm 0.004	0.3756 \pm 0.002	0.3805 \pm 0.003 (Π_2)	Narasimhan lower by 1.4 sd; intra- Π_2
FOLIO	0.7478 \pm 0.008	0.7705 \pm 0.021	0.7195 \pm 0.007 (Π_1)	ours wins (2.7/2.3 joint sd)

Table 5: Cost-sensitive adaptations of two learning-to-defer baselines (Mozannar–Sontag 2020, Narasimhan et al. 2022) evaluated under the identical strict nested 5-fold-by-5-seed CV protocol used in this paper. Numbers are mean loss \pm seed std; lower is better. Bold marks our deployable per-benchmark winner from Table 1. Both adapted L2D baselines sit firmly in Π_2 by construction, so the comparison is intra- Π_2 on HallusionBench/A-OKVQA and inter-class on FOLIO. They recover the Π_2 -class result on HallusionBench (Narasimhan ties our HGBC within 0.3 joint seed-sd; Mozannar trails by 3.6 joint seed-sd) and on A-OKVQA (Narasimhan numerically below our Selective by 1.4 joint seed-sd, intra- Π_2 variation), but trail our Π_1 winner on FOLIO by 2.7 and 2.3 joint seed-sd respectively, the variance-bounded sub-case (Cor 1 (ii)) where instance-level estimation is unreliable and partition routing is the regime-correct class. SMS-Spam is excluded because in its residual-bounded regime (Theorem 1) L2D wrappers reduce to direct by construction.

F Baselines, ablations, and CV diagnostics

F.1 Cost-sensitive learning-to-defer adaptations

As a robustness check, we instantiate families from outside our own pool and ask whether they show the same qualitative failures and successes. We run two cost-sensitive adaptations of canonical learning-to-defer baselines under the identical strict nested CV protocol: a softmax surrogate adapted from Mozannar and Sontag [Mozannar and Sontag, 2020], and a post-hoc plug-in estimator adapted from Narasimhan et al. [Narasimhan et al., 2022]. Both sit in Π_2 (instance-level learned controllers) by construction. The Mozannar variant is implemented as a row-replicated multinomial logistic regression with per-row weights $w_{i,a} = L_{\max,i} - L[i, a]$; the Narasimhan variant trains one HistGradientBoosting regressor per action $\hat{L}_a(x)$ and selects $\pi(x) = \arg \min_a \hat{L}_a(x)$ at test time. These are not drop-in reproductions of the original human-deferral objectives; they are loss-matrix-compatible implementations designed to test whether other Π_2 -style learners encounter the same regimes. We sweep a small hyperparameter grid on each ($C \in \{0.3, 1.0\}$ for Mozannar, $\max_depth \in \{3, 4\}$ for Narasimhan) and run them through the same 5-fold-by-5-seed strict CV pipeline as our own families. Table 5 reports the results.

The comparison is useful but deliberately limited. On HallusionBench ($n=920$, Bernstein-viable), Narasimhan-md3 (0.8990 \pm 0.007) ties our HGBC-md3 (0.8970 \pm 0.004) within 0.3 joint seed-sd, while Mozannar- $C=0.3$ (0.9203 \pm 0.005) trails by ≈ 3.6 joint seed-sd; the spread reflects implementation-level differences (post-hoc plug-in vs. row-replication) within a single Π_2 class, not a class-selection signal. Our Π_1 KMeans- $K=8$ (0.9093 \pm 0.003) beats Mozannar by ≈ 1.9 joint seed-sd but trails Narasimhan within ≈ 1.4 joint seed-sd, consistent with HallusionBench sitting just inside the high-signal Π_2 -favorable region. On A-OKVQA (high-signal boundary), Narasimhan-md3 reaches 0.3756 \pm 0.002, numerically below our Π_2 Selective at 0.3805 \pm 0.003 by ≈ 1.4 joint seed-sd. Both controllers are firmly Π_2 -class by construction, so this is intra- Π_2 variation rather than a class-selection signal: the canonical-pool Π_2 winner Selective and the external Π_2 implementation Narasimhan agree to within 0.005, exactly the empirical-tightness pattern Corollary 1 (iii) predicts when C_{Π_2} is the ceiling and reasonable Π_2 families realize it; Mozannar at 0.3877 shows that not every Π_2 implementation realizes the ceiling equally, an intra- Π_2 spread that does not flip the class-selection conclusion. On FOLIO (variance-bounded, $n=203 \ll n_{\min}=1898$), Mozannar- $C=1.0$ (0.7478 \pm 0.008) and Narasimhan-md3 (0.7705 \pm 0.021) trail our KMeans- $K=6$ partition at 0.7195 \pm 0.007 by ≈ 2.7 and ≈ 2.3 joint seed-sd respectively, matching the Π_1 -wins- Π_2 sub-case of Corollary 1 (ii); both L2D adaptations are Π_2 -class by construction and inherit the $n < n_{\min}^{\text{Bern}}$ uncertified-sign behaviour the theory predicts. The pattern across the three benchmarks tracks the theory: when $n \geq n_{\min}^{\text{Bern}}$, multiple independent Π_2 implementations cluster within seed noise; when $n \ll n_{\min}$, partition routers strictly dominate the Π_2 realizations we tested, including the two L2D adaptations outside our main family pool. The adapted L2D baselines are not a proof that the original L2D objectives would behave identically under every implementation choice; they show that the observed regime classification is robust beyond our HGBC family.

Benchmark	Π_0 best	KMeans Π_1 best	CART Π_1 best	verdict
HallusionBench	1.0000	0.9093 \pm 0.003	0.9104 \pm 0.004	both beat Π_0 ; tied within noise
A-OKVQA	0.4138	0.3902 \pm 0.009	0.3742 \pm 0.005	both beat Π_0 ; CART better
FOLIO	0.7520	0.7195 \pm 0.007	0.7981 \pm 0.042	KMeans wins; CART overfits

Table 6: Non-KMeans Π_1 realization: shallow CART partition routers under the identical strict nested 5-fold-by-5-seed CV protocol. Bold marks the Π_1 winner among KMeans/CART. On HallusionBench KMeans and CART tie within seed noise. On A-OKVQA CART-d4 at 0.3742 falls \approx 1.1 joint seed-sd below the canonical Π_2 winner Selective at 0.3805, an additional witness for the Cor 1 (iii) commensurate-ceiling boundary in which finite-capacity family choice can flip the empirical winner. On FOLIO, the depth-bounded tree overfits at $n=203$, consistent with Theorem 3’s required per-leaf sample budget not being met; KMeans’s fixed K acts as an implicit regularizer.

F.2 Ablations: CART partition router, loss-weight sensitivity

Two ablations probe the robustness of the regime map. The first asks whether the Π_1 winners depend on KMeans. We add a second, structurally different Π_1 realization: a shallow CART partition router (`DecisionTreeClassifier` at `max_depth` \in $\{3, 4\}$) whose splits are fit on the per-sample loss-argmin label and whose leaves are re-assigned the cell-wise loss-argmin action at fit time (Appendix C.3). Table 6 reports the per-benchmark numbers. On HallusionBench, KMeans- $K=8$ (0.9093) and CART-d4 (0.9104) tie within seed noise, both losing to the per-class Π_2 winner, so HallusionBench remains a clean Π_2 win regardless of partition method. On A-OKVQA the picture is more interesting: CART-d4 reaches 0.3742 ± 0.005 , numerically below the canonical Π_2 Selective at 0.3805 ± 0.003 by \approx 1.1 joint seed-sd. This is within seed noise, so we retain Selective as the canonical Π_2 winner because the canonical pool is fixed in advance, but the CART ablation places A-OKVQA’s deployable-class outcome in a Π_1/Π_2 tie rather than a clean Π_2 win, sharpening the body’s reading of A-OKVQA as the Cor 1 (iii) ceiling-comparison boundary. It is exactly the second clause of the corollary at work: when C_{Π_1} and C_{Π_2} are commensurate, finite-capacity family realization—here the choice between an axis-aligned CART and a centroid-based KMeans—can flip the empirical winner between supportable adaptive classes. On FOLIO the depth-bounded CART overfits at $n=203$ and lands at 0.7981 ± 0.042 , $+0.046$ worse than Π_0 ; KMeans- $K=6$ at 0.7195 remains the Π_1 winner. CART’s FOLIO failure is the partition-router-side analogue of Cor 1 (ii)’s Π_2 failure: at $n=203$, depth-3-or-4 CART leaves carry too few samples for the empirical per-leaf argmin to track its cell-best action, consistent with the per-leaf sample budget required by Theorem 3 not being met; KMeans’s fixed K is an implicit regularizer that the depth-bounded tree, with its more flexible leaf structure, lacks.

The second ablation addresses the cost-sensitivity of the combined loss. Classical reject-option and cost-sensitive evaluation explicitly depend on operating costs [Chow, 2003, Drummond and Holte, 2006], so a class-selection result should not hinge on a single arbitrary weight vector. We therefore rerun the deployable $\Pi_0/\Pi_1/\Pi_2$ family pool under seven local perturbations of the canonical core weights: (1, 1, 0.05), correctness weight 0.75 and 1.25, risk weight 0.75 and 1.25, and cost weight 0.025 and 0.10, always with the same strict 5-fold-by-5-seed protocol. Table 7 summarizes the winner counts. Two of the three benchmarks are fully stable: A-OKVQA Π_2 (7/7) and FOLIO Π_1 (7/7). HallusionBench is the boundary case: the canonical-weights winner is Π_2 (5/7), but two perturbations (`correct_high`, `risk_low`) swap the winner to Π_1 by less than 0.005, reflecting the fact that the canonical-weights gap between Π_1 (KM- $K=8$ at 0.909) and Π_2 (HGBC-md3 at 0.897) is only \approx 3 seed-sd of Π_2 . The qualitative regime map is therefore robust on A-OKVQA and FOLIO, with HallusionBench’s Π_1/Π_2 boundary slightly weight-dependent: the operating-cost neighborhood swept here, which spans $\pm 25\%$ perturbations of the correctness and risk weights and a $2\times$ range of cost weights around the canonical setting, leaves the deployable winner unchanged on A-OKVQA and FOLIO but flips it on HallusionBench in two of seven variants—a quantitative confirmation that HallusionBench sits on the Π_1/Π_2 ceiling-comparison boundary predicted by Corollary 1 (iii).

F.3 Automated class selection

Automated inner-CV class selection is near-best on the two Bernstein-viable benchmarks and predictably fails on FOLIO without the regime-theoretic class restriction. Strict nested auto-pick loss

Benchmark	canonical class	winner counts over 7 weights	min winner margin	interpretation
HallusionBench	Π_2	$\Pi_2:5, \Pi_1:2$	0.0047	Π_1/Π_2 boundary
A-OKVQA	Π_2	$\Pi_2:7$	0.0049	stable Π_2
FOLIO	Π_1	$\Pi_1:7$	0.0074	stable Π_1

Table 7: Loss-weight sensitivity on the three benchmarks where adaptive controllers are theoretically viable (SMS-Spam excluded as residual-bounded). We rerun the deployable $\Pi_0/\Pi_1/\Pi_2$ family pool under strict 5-fold-by-5-seed CV for seven local perturbations of the canonical weights (1, 1, 0.05). The HallusionBench Π_1/Π_2 boundary is itself a quantitative diagnostic: under the canonical weights Π_2 edges Π_1 by only ≈ 3 seed-sd, and two perturbations swap the winner. A-OKVQA and FOLIO are fully stable across the seven variants, with FOLIO’s 0.0074 minimum margin reflecting its 4.5 seed-sd canonical Π_1 gap.

differences relative to `always_direct` are $\Delta \in \{-0.183, -0.028, -0.003\}$ on {HallusionBench, A-OKVQA, FOLIO}. On HallusionBench the auto-pick lands within seed noise of the per-class Π_2 winner ($\Delta = -0.183$ vs. per-class Π_2 winner $\Delta = -0.188$, 0.7 joint seed-sd), and A-OKVQA remains close but more borderline ($\Delta = -0.028$ vs. per-class Π_2 winner $\Delta = -0.033$, 1.4 joint seed-sd). On FOLIO, the auto-pick reaches only $\Delta = -0.003$, materially below the per-class Π_1 winner at $\Delta = -0.033$ (a 0.030 absolute-loss gap, or 1.7 joint seed-sd when auto-pick variability is included) because at $n=203$ the unrestricted inner-CV pool occasionally lands on Π_2 families whose sign Theorem 2 explicitly does not certify. This is exactly the failure mode Corollary 1 (ii) predicts when $n < n_{\min}^{\text{Bern}}$: empirical CV alone cannot reliably separate Π_1 from Π_2 , and the regime diagnostic is what supplies the missing class restriction. The same per-fold class shares (19/25 Π_1 , 4/25 Π_2 , 2/25 Π_0) make this concrete: 4 outer-folds pick a Π_2 family at coverage q where Theorem 2 does not certify the sign, and these 4 folds are what drag the auto-pick mean from the per-class Π_1 winner to the much smaller -0.003 . Restricting the candidate pool with the regime diagnostic ($\beta > 0, n < n_{\min}^{\text{Bern}} \Rightarrow$ exclude Π_2 per Cor 1 (ii)) would force those 4 Π_2 folds to be reselected from $\Pi_0 \cup \Pi_1$, removing the uncertified instance-level choices and steering selection toward the regime-correct Π_1 -dominated pool. *HallusionBench* picks Π_2 HGBC on 20/25 outer-folds (HGBC-md4 on 12/25, HGBC-md3 on 8/25) and Π_1 KMeans on the remaining 5/25, consistent with the per-class Π_2 winner in Table 1. *FOLIO* picks Π_1 KMeans on 19/25 outer-folds (KM- $K=6$ on 6/25, KM- $K=8$ on 5/25, KM- $K=4$ and $K=5$ on 4/25 each), the Π_2 family Selective- $C=0.3$ on 4/25, and Π_0 `always_direct` on 2/25; this dominant Π_1 class share matches the deployable per-class winner. *A-OKVQA* is the one benchmark where the inner-CV class selection is ambiguous: 10/25 outer-folds pick the Π_1 winner KMeans- $K=4$ while the remaining 15/25 are distributed across three Π_2 families (Selective $C=0.3$ on 10/25, HGBC-md3 on 4/25, HGBC-md4 on 1/25), giving a 10:15 $\Pi_1:\Pi_2$ class split with the resulting auto-pick loss falling between the two per-class winners. This is precisely the high-signal Π_1/Π_2 boundary case predicted by Corollary 1 item (iii) when the Π_1 and Π_2 ceilings are commensurate; the per-class decomposition on outer-train remains a more informative summary than the inner-CV argmin in this regime. On TextVQA-OCR, the per-class decomposition selects Π_3 as the deployable top-rung winner because the OCR channel is available at prediction time. If the non-deployable A-OKVQA gold-rationale oracle is included in the candidate pool, inner-CV also selects it; we report that only as the oracle experiment of Appendix D.4, not as the deployable auto-pick result.